Space-time extreme wind waves: Analysis and prediction of shape and height

BenetazzoAlvise[a] BarbariolFrancesco[a] BergamascoFilippo[b] CarnielSandro[a] SclavoMauro[a]
https://doi.org/10.1016/j.ocemod.2017.03.010

Abstract

In this study, we present the analysis of the temporal profile and height of space-time (ST) extreme wind waves. Wave data were gathered from an observational ST sample of sea surface elevations collected during an active sea state, and they were examined to detect the highest waves (exceeding the rogue wave threshold) of specific 3D wave groups close to the apex of their development. Two different investigations are conducted. Firstly, local maximum elevations of the groups are examined within the framework of statistical models for ST extreme waves, and compared with observations and predictions of maxima derived by one-point time series of sea surface elevations. Secondly, the temporal profile near the maximum wave crests is analyzed and compared with the expectations of the linear and second-order nonlinear extension of the Quasi-Determinism (QD) theory. Our goal is to verify, with real sea data, to what extent, one can estimate the shape and the crest-to-trough height of near-focusing large 3D wave groups using the QD and ST extreme model results. From this study, it emerges that the elevations close to the crest apex are narrowly distributed around a mean profile, whilst a larger dispersion is observed away from the maximum elevation. Yet the QD model furnishes, on average, a fair prediction of the maximum wave heights, especially when nonlinearities are taken into account. Moreover, we discuss how the combination of ST extreme and QD model predictions allows establishing, for a given sea condition, the portrait of waves with very large crest height. Our results show that these theories have the potential to be implemented in a numerical spectral model for wave extreme prediction.

1. Introduction

Extreme oceanic surface waves are topical for scientist, mariners and engineers (Muller et al., 2005). Indeed, their relevance and apparently elusive nature make extreme waves a well-studied topic by pure and applied researchers. In the oceanographic community, extreme waves are often referred to as “rogue” or “freak” (a notion which was first introduced by Draper, 1965) when the crest-to-trough height H is at least about twice the significant wave height H_s, or the crest height exceeds $1.25H_s$ (Dysthe et al., 2008, Kharif et al., 2009). For the simplest case of linear waves with infinitively narrow spectrum, the occurrence probability of rogue waves is rather small (a rogue wave with $H > 2H_s$ should appear on average once among about 3000 individual waves), and for a given sea state the theory fails to predict the probability of waves much larger than those in the surrounding field. Generally, rogue waves appear in a wave record apparently out of nowhere in small groups either singly (Gemmrich and Garrett, 2008, Kharif et al., 2009). The use of theoretical models that deviate from linearity increases the understanding of the occurrence and magnitude of extreme events for two principal mechanisms. First, waves with finite amplitude generate second- and higher-order nonlinearities that make wave crests sharper and higher (Forristall, 2000, Sharma and Dean, 1979, Tayfun, 1980). Second, considerable deviations from linearity are also given by nonlinear four-wave interaction that produces, under certain circumstances, very large waves in such a way that extreme events become more likely (Janssen, 2003, Onorato et al., 2013, Onorato et al., 2001). By analyzing a large dataset of field measurements, Christou and Ewans (2014) provided evidence that rogue waves are not directly governed by sea state parameters, and at the time of the rogue wave event almost all frequency components with nonzero spectral values are approximately in phase with each other. Nonlinearities are also responsible of changes in the dynamics of large wave groups (Adcock et al., 2015).

In addition to non-Gaussian sea conditions, large probabilities of occurrence of very high waves are attained when the statistics applied to one-point observations is extended to incorporate the probability that maxima occur over a specific sea surface region. The statistical distribution of maximum sea surface elevations over a spatial or spatio-temporal (ST) domain is thereby derived (Fedele, 2012, Krogstad et al., 2004). This approach considers the sea surface elevation as a multi-dimensional (2D space + time) Gaussian field, whose probability of maxima

is linked to the geometrical and statistical properties of the ST field, according to the Piterbarg's theorem (Piterbarg, 1996) or the Euler Characteristic approach (Adler and Taylor, 2007, Adler, 2000). ST extreme stochastic model results have been assessed and discussed using numerical (Barbariol et al., 2015, Krogstad et al., 2004, Socquet-Juglard et al., 2005) and observational data (Benetazzo et al., 2015, Fedele et al., 2013), and extended to incorporate weakly nonlinear waves by Socquet-Juglard et al., 2005, Fedele et al., 2013, and Benetazzo et al., (2015). More recently, Fedele (2015) confirmed that in the ST models the second-order nonlinearities cannot be neglected, while it is expected a modest contribution due to third-order nonlinearities. The ST extreme model based on the Euler Characteristic technique will be used in this study to characterize the maximum elevations of specific 3D wave groups close to the apex of their development. Indeed, there is a close connection between ST maxima and spatio-temporal modulation of unsteady and dispersive wave groups (Boccotti, 2000, Fedele et al., 2013). In particular surface elevations around the maximum wave crests can be derived by the shape of specific 3D wave groups whose apex occurs at time and position of the crest itself. In this study we use the principal results of the Quasi-Determinism (QD) theory (Boccotti, 2000, Boccotti, 1983) that predicts the ST Gaussian free surface displacement and the velocity potential around a large wave occurring at a fixed time and location. There are two versions of the QD theory: the first version (used in this study) analyzes the ST shape of wave groups reaching a maximum crest elevation, while the second version emphasizes on the shape when the groups experience the maximum wave height. The two forms of the QD are consistent with each other as they reveal that the two extreme states are specific conditions of well-defined ST wave groups. As important corollaries of the QD theory, Boccotti (2000) derived the asymptotic form of the probability distribution of wave heights (generalized for nonlinear waves by Alkhalidi and Tayfun, 2013), and characteristic periods of the highest waves in a sea state with a given energy spectrum. Both formulations of the QD theory were extended to second-order in the Stokes expansion by Arena (2005) and Fedele and Arena (2005). The QD theory was verified in different small-scale field experiments with undisturbed waves (Boccotti et al., 1993b) and waves interacting with structures (Boccotti et al., 1993a), but a thorough assessment using open sea data is still missing. However, scholars have already used the QD model results to characterize the shape of rogue waves. For example, this model has been corrected up to fifth-order

by Walker et al., (2004) to clarify the magnitude and character of the nonlinear contributions in describing the shape of the Draupner "New Year" rogue wave (Haver, 2004). Walker et al., (2004) found that nonlinear contributions decrease rapidly as the order increases, and that effects of nonlinearity are more pronounced close to the apex of a crest.

In this study, the QD theory, at first- and second-order of approximation, has been used to investigate the shape of observed extreme waves, and obtain, as corollary, a predictive framework for their wave height H. Predictions of the ST and QD models are evaluated using real wave data recorded by means of a stereo wave imaging system (namely Wave Acquisition Stereo System, WASS; Benetazzo, 2006, Benetazzo et al., 2012) installed on an offshore oceanographic research platform in the northern Adriatic Sea (Italy). Space-time sea surface elevation fields were collected during an active sea state, and analyzed to extract time records at the spatial positions where the ST wave groups were close to the apex of their development stage (Benetazzo et al., 2015). We selected only groups whose maximum crest height exceeded the threshold $1.25H_s$, thus obtaining a sample of 23 rogue waves. These represent the sample used for our analysis. We review main results of QD and ST extreme theories aimed at improving (supported by field measurements) the link between them, attempting to define a predictive framework for the shape and height of large waves in a sea state with given directional energy spectrum.

The paper is organized as follows. In Section 2.1 we summarize and discuss main characteristics of the QD model for linear and second-order nonlinear wave fields. Moreover, results of the theory are used to derive an expectation of the crest-to-trough height of maximum waves. Section 2.2 describes the statistical model of ST extreme waves resulting in nonlinear sea surface elevation fields, which were measured in open sea using a stereo wave imaging system (Section 3). The latter are used to assess ST extreme wave predictions, which are also compared with outcomes of time-based statistical theories for wave extremes. In Section 4, results from QD and ST models are used to analyze the height and the temporal profile of extreme waves detected by the stereo system; results of both models are then combined in a framework to predict the profile and height of very high waves. Last section summarizes main findings of the study.

2. Theoretical framework

2.1. Expected shape and height of large waves

2.1.1. Gaussian wave fields

In this section we analyze and discuss basic elements of the QD theory for the general case of a Gaussian 3D random wave field with a given directional energy distribution. Let the sea surface elevation field, with zero-mean and standard deviation σ, be $\eta_1(x, y, t) = \eta_1(\boldsymbol{x}, t)$, where η_1 is the Gaussian component of the field $\eta(x, y, t)$, $\boldsymbol{x} = (x, y)$ denotes the horizontal coordinate vector, and t the time. Next, let $\eta_{1cm} = \max\{\eta_1(\boldsymbol{x}_0, t_0)\}$ represent the elevation of a local wave maximum (crest) occurring at the horizontal position $\boldsymbol{x}_0 = (x_0, y_0)$ and instant $t = t_0$, such that the sea surface gradient $\nabla\eta_1(x_0, y_0, t_0) = 0$. Now we denote by $\boldsymbol{X} = (X, Y)$ the 2D horizontal vector measured from $\boldsymbol{x}_0$, and τ the time lag from t_0. In the finite coordinates $\boldsymbol{X}$ and τ the ST autocovariance function of $\eta_1(\boldsymbol{x},t)$ is given by(1)ψ1(X,τ)=E{η1(x0,t0)η1(x0+X,t0+τ)}where E{} denotes expectation.
The QD model predicts that the sea surface elevation field surrounding the maximum wave crest is that of a stochastic ST wave group whose conditional mean surface profile η¯1($\boldsymbol{X}$, τ) is given by (Boccotti, 2000, Boccotti, 1983, Lindgren, 1972, Lindgren, 1970, Slepian, 1962)(2)η¯1(X,τ)=E{η1(x0+X,t0+τ)|η1(x0,t0)=η1cm}=η¯1,det+R1(X,τ)where(3)η¯1,det=η1cmψ1(X,τ)σ2is of $O(\eta_{1cm})$ and denotes the deterministic part of the process. The other way around, a large wave crest, with height η_{1cm}, occurs where and when the wave is at its maximum elevation within a linear 3D group (with mean ST shape η¯1,det, shown, for instance, in Fig. 1) that evolves over background random waves represented by $R_1(\boldsymbol{X}, \tau)$. The residual $R_1(\boldsymbol{X}, \tau)$ is Gaussian, with E{$R_1(\boldsymbol{X}, \tau)$} = 0, and it is of O(η1cm0), and it will be neglected in the following analysis. The variance of the profile is a function of ($\boldsymbol{X}$, τ), it attains its minimum at ($\boldsymbol{x}_0$, t_0), and it is smaller for higher wave crests. In fact, the random ST sea surface shape around η_{1cm} tends asymptotically (with probability approaching 1) to the deterministic profile η¯1($\boldsymbol{X}$, τ) as the normalized crest height $\eta_{1cm} / \sigma \rightarrow \infty$ (i.e. the crest is very high with respect to the mean crest height).

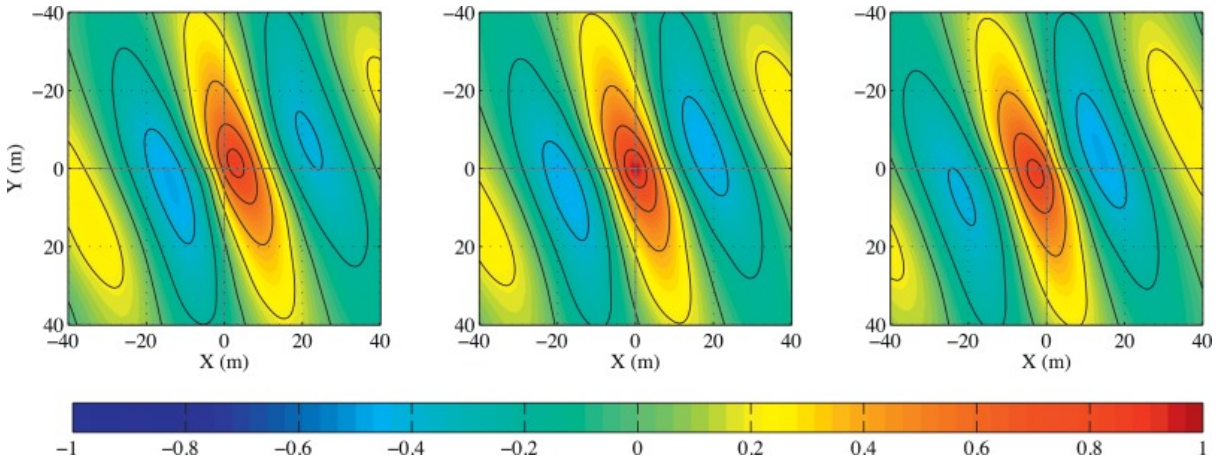

Fig. 1. Space-time shape of a large linear wave group. Normalized elevation $\psi_1(\boldsymbol{X}, \tau)/\sigma^2$ at three instants: $\tau = -0.1T_p$ (growth stage; left panel), $\tau = 0$ (focusing point; middle panel), and $\tau = +0.1T_p$ (decay stage; right panel). Direction of wave propagation is from top-right to bottom-left. Sea surface elevation isolines are drawn at 0.2 interval. The ST autocovariance function and the peak period T_p are determined using the observed directional wave spectrum shown in Fig. 5. For comparison see also Fig. 1. of Adcock and Draper (2015).

For oceanographic applications we take advantage of the pairing (via Fourier transform) between the angular frequency (ω) - direction (θ) wave spectrum $S(\omega, \theta)$ and the autocovariance function $\psi_1(\boldsymbol{X}, \tau)$, which can be written as follows (Boccotti, 2000)(4)ψ1(X,t)=∫ω∫θS(ω,θ)cos(k·X−ωτ)dωdθwhere $\boldsymbol{k} = (k_x, k_y) = (k\cos\theta, k\sin\theta)$ is the wavenumber vector associated with ω and θ via the linear dispersion relation for gravity waves.

The autocovariance function attains its global maximum at coordinates $\boldsymbol{X} = (0, 0)$ and time $\tau = 0$, where it coincides with the zero-th order moment of the spectrum given by(5)ψ1(0,0,0)=∫ω∫θS(ω,θ)dωdθ=σ2

Since scholars usually deal with time records of sea surface elevations, it is interesting to obtain the shape of the group η¯1,det evolving over time only. As it can be seen by Eq. (2), the temporal profile of the ST wave group depends on the displacement $\boldsymbol{X}$ from the position $\boldsymbol{x}_0$. In the special case $\boldsymbol{X} = (0, 0)$, i.e. where the group is at the apex of its development, the temporal profile of the large wave (see Fig. 2) is given by(6)η¯1(τ)=E{η1(x0,t0+τ)|η1(x0,t0)=η1cm}=η1cmE{η1(x0,t0)η1(x0,t0+τ)}σ2=η1cmψ1(τ)σ2where the autocovariance function $\psi_1(\tau)$ can be expressed by means of spectral integral quantities as(7)ψ1(τ)=ψ1(0,0,τ)=∫ω∫θS(ω,θ)cos(ωτ)dωdθ=∫ωS(ω)cos(ωτ)dωand the omni-directional frequency spectrum $S(\omega)$ is given by(8)S(ω)=∫θS(ω,θ)dθ

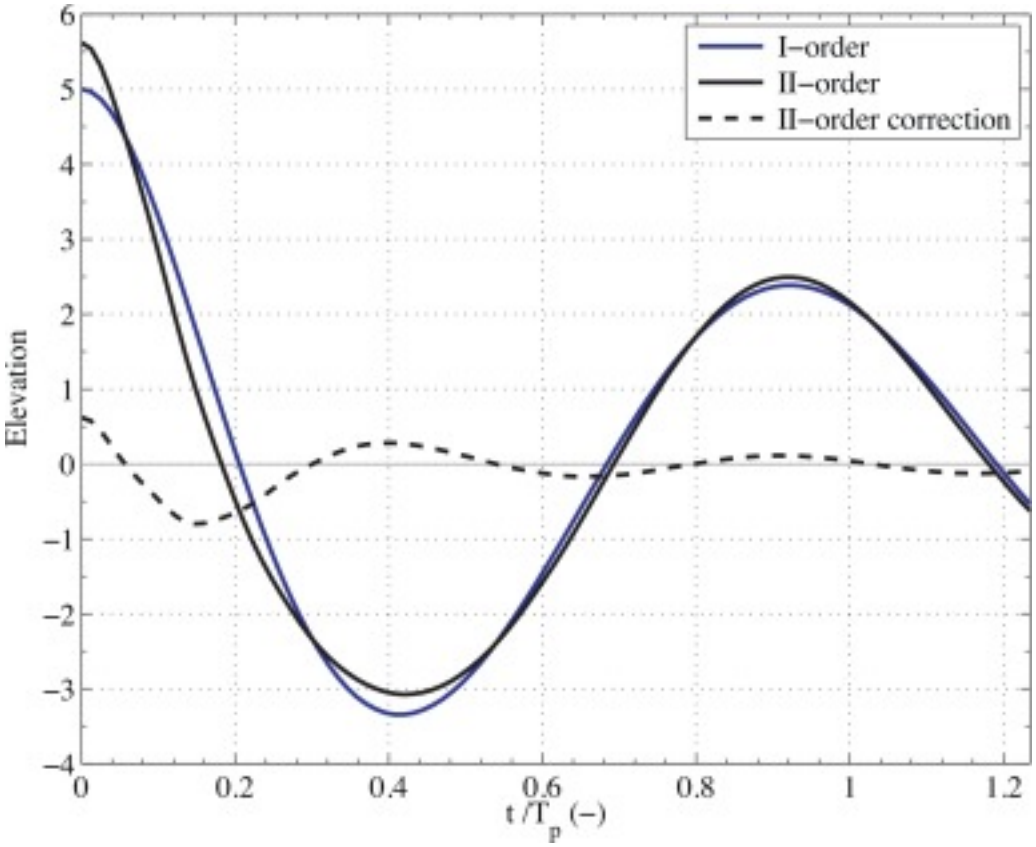

Fig. 2. Temporal shape of a large wave group at the focusing point $\boldsymbol{X} = (0, 0)$ near a crest with linear height $\eta_{1cm} = 5\sigma = 1.25H_s$. Mean linear profile $\bar{\eta}1$(I-order), mean second-order nonlinear profile $\bar{\eta}2$(II-order), and second-order nonlinear correction. In Figure, the time lag τ is indicated with the time axis t, and $t_0 = 0$. All profiles and the peak period T_p (used to scale t) are determined using the wave spectra shown in Fig. 5.

It is worth noting that for one-point wave records at sea (e.g. collected with wave gauges or buoys) the position $\boldsymbol{X}$ is not determined. Consequently, it is not possible to derive the theoretical temporal profile of very high waves at coordinates $(\boldsymbol{x}_0 + \boldsymbol{X})$, so that it can ben compared, for instance, with observations. This has consequences for the interpretation of QD model results, as we shall see in Section 4.

2.1.2. Second-order nonlinear wave fields

It is well known that the inclusion of nonlinearities modifies the theoretical shape of linear sea waves (Longuet-Higgins, 1963). Second-order nonlinearities due to bound harmonics (i.e., harmonics that do not satisfy the linear dispersion relation for gravity sea waves) displace upward crest heights and trough elevations, and generate wave crest steeper than the linear counterpart (Fig. 2). As a consequence,

the probability density function of sea surface elevations is skewed to the negative values, and the skewness coefficient of η (equal to zero for Gaussian fields) is positive. For weakly nonlinear random seas, the second-order sea surface elevation field η_2 can be described by the nonlinear mapping (Longuet-Higgins, 1963, Sharma and Dean, 1979)(9)η2=η1+η1−2where η_{1-2} is the second-order nonlinear correction to the linear elevation η_1. Under general conditions in deep and transitional water depths, the extension of the time-dependent conditional process (6) to include the role of second-order bound nonlinearities is given by (Arena, 2005, Fedele and Arena, 2005, Fedele and Tayfun, 2009)(10)η¯2(τ)=E{η2(x0,t0+τ)|η2(x0,t0)=η2cm}=η1cmψ1(τ)σ2+16η1cm2λ(τ)σ4=η¯1(x0,t0+τ)+16η1cm2λ(τ)σ4where η¯2 is the mean nonlinear temporal profile (Fig. 2), and η_{2cm} is the second-order nonlinear crest height occurring at the position $\boldsymbol{x}_0$ and instant t_0.

In Eq. (10) the term 16η1cm2λ(τ)σ4 is the nonlinear correction to the linear shape, and the function $\lambda(\tau)$ is expressed as (Tayfun and Fedele, 2007)(11)λ(τ)=3E{η12(x0,t0)η1−2(x0,t0+τ)}=32∫ki∫kjS(ki)S(kj)[K+cosϕ++K−cosϕ−]dkidkj where $\phi^+ = (\omega_i + \omega_j)\tau$, $\phi^- = (\omega_i - \omega_j)\tau$, and $S(k)$ is the omnidirectional wavenumber spectrum, which can be estimated using the Fourier transform of the 3D wave field (Banner et al., 1989, Benetazzo et al., 2016, Hwang et al., 2000, Romero and Melville, 2010), or, alternatively, evaluated from $S(\omega)$ using the following conversion(12)S(k)=S(ω)dωdk

The interaction terms K^+ and K^- (which are function of the harmonics' frequency and the water depth; Sharma and Dean, 1979) relate to the second-order bound harmonics with frequencies $(\omega_i + \omega_j)$ and $(\omega_i - \omega_j)$, respectively, and produce, on the one hand, higher wave crests and shallower wave troughs, and, on the other, set-down of the mean sea level under the wave groups.

We note that at the wave group focusing instant (i.e. $\tau = 0$) Eq. (11) yields(13)λ(0)=3E{η12(x0,t0)η1−2(x0,t0)}=32∫∫S(ki)S(kj)[K++K−]dkidkjwhere $\lambda(0)$ is related to the skewness coefficient λ_3 of η_2 as follows (Fedele and Tayfun, 2009, Janssen, 2009, Tayfun, 1986)(14)λ(0)=3E{η12η1−2}≈E{η23}=λ3σ3≥0which is therefore $\lambda(0) = \lambda_3\sigma^3 = 0$ for linear waves. For zero time-lag, Eq. (10) yields(15)η2cm=η1cm+12λ33η1cm2σconsistent to the Tayfun equation (Tayfun, 1980), and indicating that the nonlinear crest height is a quadratic function of the linear component. It is worth noting that in Eq. (10) first- and second-order wave group maxima are phase-locked (Fedele, 2008), in a way that a large crest (with

elevation η_{1cm}) of a linear wave occurs simultaneously with its second-order extension (with elevation η_{2cm}). In other words, the nonlinear surface surrounding locally a large crest is function of the Gaussian wave group (Fedele and Tayfun, 2009). For narrowband and long-crested waves in deep waters the second-order nonlinear correction to $\eta^{-}1$can be expressed as function of the Hilbert transform of η_1 with respect to time (Tayfun, 1986, Tayfun, 1980).

2.1.3. Height of large waves

At the wave group focusing point $\boldsymbol{X} = (0, 0)$, linear and second-order nonlinear QD models can be used to derive an expectation, on the time domain, of the crest-to-trough height of the wave with maximum crest height. The abscissa τ^* of the first minimum (trough) of $\psi_1(\tau)$ is related to the mean period of the highest waves of a sea state with a given energy spectrum (Boccotti, 1983). As a consequence, the expected height ($H^{-}1cm$) of the wave with (large) crest elevation η_{1cm} can be analytically derived from $\eta^{-}1(\tau)$ in the following form(16)$H^{-}1cm=\eta 1cm(1-\psi 1^*)$where $\psi 1^* = \psi_1(\tau^*) / \sigma^2 \in [-1\ 0)$ is the value of the first minimum of the autocovariance function, and $\eta_{1cm}\psi 1^* < 0$ is the mean displacement of the linear wave trough preceding or following η_{1cm}. Boccotti (2000) demonstrated that, for a given linear group, $H^{-}1cm$ is smaller than the expected value of the maximum wave height ($H^{-}1m$). If we assume $\eta_{1\,cm}$ corresponding to the maximum crest height in a sequence of waves (as we shall do in Section 4), wave heights $H^{-}1cm$ and $H^{-}1m$are linked by the following relationship (Boccotti, 2000)(17)$H^{-}1m=H^{-}1cm2(1-\psi 1^*)1-\psi 1^*$
The ratio $r_H = H^{-}1m/H^{-}1cm$ is larger than 1 when $\psi 1^* > -1$, and it becomes $r_H = 1$ only if $\psi 1^* = -1$, that is, the height of the wave with the maximum crest corresponds to the maximum wave height if the wave spectrum is infinitely narrow (in this respect $\psi 1^*$ is interpreted as a narrow-bandedness parameter of the wave spectrum; Boccotti, 2000).
The effect on the wave height $H^{-}1cm$ of second-order nonlinearities is generally small, particularly in narrow band seas (Tayfun and Fedele, 2007). Notwithstanding, in the general case, the expected height ($H^{-}2cm$) of the wave with second-order nonlinear crest elevation η_{2cm} can be derived using the relationship (10) as follows(18)$H^{-}2cm=[\eta 1cm+\lambda(0)6\sigma 4\eta 1cm2]-[\eta 1cm\psi 1^*+\lambda^*6\sigma 4\eta 1cm2]=\eta 1cm(1-\psi 1^*)+\lambda(0)-\lambda^*6\sigma 4\eta 1cm2=H^{-}1cm+\beta H^{-}1cm2$where $\lambda^* = \lambda(\tau^*)$, and(19)$\beta=1(1-\psi 1^*)2\lambda(0)-\lambda^*6\sigma 4$

2.2. Space-time extreme crest heights

In stormy seas, maximum sea surface elevations belong to specific wave groups (Longuet-Higgins, 1984) reaching their maximum development at different spatial positions and times. Benetazzo et al., (2015) shown that these maximum elevations are predicted using a stochastic model for nonlinear ST extremes. Here basic elements of that model are described, focusing our interest on the statistical structure of wind sea extreme waves at short-term time intervals (~1 to 3 hours). The variable of interest is the sea surface elevation η (measured vertically from the mean sea plane and pointing upward) which is represented as a multi-dimensional random field in $\Re^3$, evolving over time t and Cartesian horizontal coordinates x and y, viz.(20)η=η(x,y,t)
The purpose is to obtain a formulation for the probability of exceedance of maximum elevations of the stochastic process (20), and a prediction of the global maximum $\eta_{STm} = \max\{\eta(x, y, t)\}$ over a bounded ST region $U \in \Re^3$, delimited by a time duration and a 2D spatial region (see for example the region depicted in Fig. 1 of Fedele, 2012). The sea state over U is assumed to be statistically stationary in time and homogeneous in space.

2.2.1. The Euler Characteristic approach for Gaussian waves

Let η_1 be the linear component of the ST random process η, with $\eta_{1STm} = \max\{\eta_1(x, y, t)\}$, and P_{1STm} the probability that the maximum elevation exceeds the threshold z over the multidimensional compact region $U \in \Re^3$(21)P1STm=Pr{η1STm>z|(x,y,t)∈U}
Adler (2000) developed a framework for handling the excursion sets defined as(22)SU,z={(x,y,t)∈U:η1(x,y,t)>z}which is the portion of the region U where the random variable η_1 exceeds the level z. A topologic invariant of $S_{U,z}$ is the so-called Euler Characteristics (hereinafter EC; a concept named after Leonard Euler, see also Worsley, 1996), which is a property that links vertices (corners), edges, and faces of $S_{U,z}$. For a generic value of z, a closed solution of the mean value of EC of the excursion set for Gaussian random fields η_1 defined in $\Re^N$ is given by (Adler, 2000 and Adler and Taylor, 2007)(23)E{EC(SU,z)}=|U|detΛ(2π)(N+1)/2σNHN−1(zσ)exp(−z22σ2)where $|U|$ is the volume of $U \in \Re^N$, and Λ is the covariance matrix of the sea surface elevation

gradient vector $\nabla\eta_1$. The function H_{N-1} in Eq. (23) is the Hermite polynomial given by(24)Hn(zσ)=n!∑j=0|n/2|(−1)jj!(n−2j)!2j(zσ)n−2j
It is interesting to note as for $N = 1$ the formula (23) reduces to the Rice's solution (Rice, 1954) that gives, in a time record, the mean number of upcrossings of the specific level z.
Adler and Taylor (2007) proved the fundamental result that for large values of the level z (i.e. $z \gg \sigma$) the probability of exceedance (21) is approximated by the expected value of EC (23). That is,(25)P1STm≈E{EC(SU,z)}as it was verified for spatial sea wave data by Fedele et al., (2012). The probability of exceedance of ST extremal waves is therefore measured by the mean EC in $\Re^3$, thus easing the calculation of P_{1STm} (see Appendix A) and, as we shall see, making the EC approach relevant for oceanographic applications.

2.2.2. An extension for second-order nonlinear waves

We consider here the random wave field as a weakly nonlinear process. If second-order nonlinearities are dominant, the key parameter to describe their effect on waves is the skewness coefficient, which affects both the wave shape and the statistics of wave crests and troughs. In particular the nonlinear processes distort the shape of the wave profile that results with crests higher and sharper and troughs shallower and flatter. Consequently, the crest height distribution function in a wave record deviates from the Rayleigh's distribution, and it is well described by the Tayfun (1980) model. According to the latter and following Benetazzo et al. (2015) the probability of exceedance P_{2STm} of second-order nonlinear ST extremes over the region U is approximated as follows(26)P2STm=Pr{η2STm>z2|U}={N3[(z1σ)2−1]+N2z1σ+N1}PR(z1)where η_{2STm} is the maximum nonlinear elevation; N_3, N_2 and N_1 are proportional to the average number of 3D, 2D, and 1D waves within U, respectively (see Appendix A for the definition of these parameters), and P_R is the Rayleigh probability of exceedance of crest heights (Longuet-Higgins, 1952). The nonlinear elevation z_2 satisfies the quadratic equation (Tayfun, 1980)(27)z2=z1+μ2z12σ>z1where μ is a measure of the wave steepness (related to the skewness coefficient), and z_1 is the linear elevation. For oceanic wave in deep waters in order to make the Tayfun model more accurate for applications, Fedele and Tayfun (2009) modified the definition of steepness parameter suggesting the following form(28)μ=μa(1−ν+ν2)where(29)μa=σka=σωa2/g=σ(m001/m000)2/gis an integral

measure of the wave steepness, ν=m000m002/m0012−1 is the spectral bandwidth (Longuet-Higgins, 1975), and m_{ijl} are the moments of the directional wave spectrum $S(\omega, \theta)$ (see Appendix A).
Approximating the right tail of P_{2STm} with a Gumbel distribution, the expected value of η_{2STm} is expressed as (Benetazzo et al., 2015)(30)η¯2STm=E{η2STm}=σh¯2STm≈σ[(h1+μ2h12)+γ(h1−2N3h1+N2N3h12+N2h1+N1)−1(1+μh1)]where h_1 is normalized mode of the probability function of linear ST extremes (see Appendix A). The expected maximum was derived by Fedele et al., (2013) for spatial nonlinear wave fields. The intensity function α_2 of the nonlinear distribution is given by(31)α2=(h1−2N3h1+N2N3h12+N2h1+N1)/(1+μh1)and the standard deviation of η_{2STm} is evaluated as(32)σ2m=σπ6α2=σπ6(h1−2N3h1+N2N3h12+N2h1+N1)−1(1+μh1)
Eq. (30) can be rewritten as(33)η¯2STm/σ=h¯2STm=(h1+μ2h12)+γα1(1+μh1)=(h1+γα1)+(μ2h12+γα1μh1)=h¯1STm+μ2(h12+γα12h1)=h¯1STm+μ2[h¯1STm2−(γα1)2]=(h¯1STm+μ2h¯1STm2)−μ2(γα1)2which shows the dependence of the nonlinear extreme crest on its linear approximation. In particular, the first term (h¯1STm+μ2h¯1STm2) is the second-order nonlinear maximum elevation computed via the Tayfun quadratic form (27) applied to the linear ST extreme elevation h¯1STm (see Appendix A). The second term μ2(γα1)2is orders of magnitude smaller than the first one as the probability density function of extremes is generally rather narrow (Gumbel, 1958, Holthuijsen, 2008), thus the ratio (γα1)2≪ 1. For instance the stormy sea state described in Benetazzo et al. (2015) had μ2(γα1)2= 0.0007.

3. Observation of extreme waves

3.1. The sample of ST wave fields

In this study, we analyze maximum waves of a sea surface elevation sample $\eta(x, y, t)$ obtained by processing a stereo-image sequence provided by an imaging system mounted on the “Acqua Alta” oceanographic research platform (northern Adriatic Sea, Italy; Fig. 3).

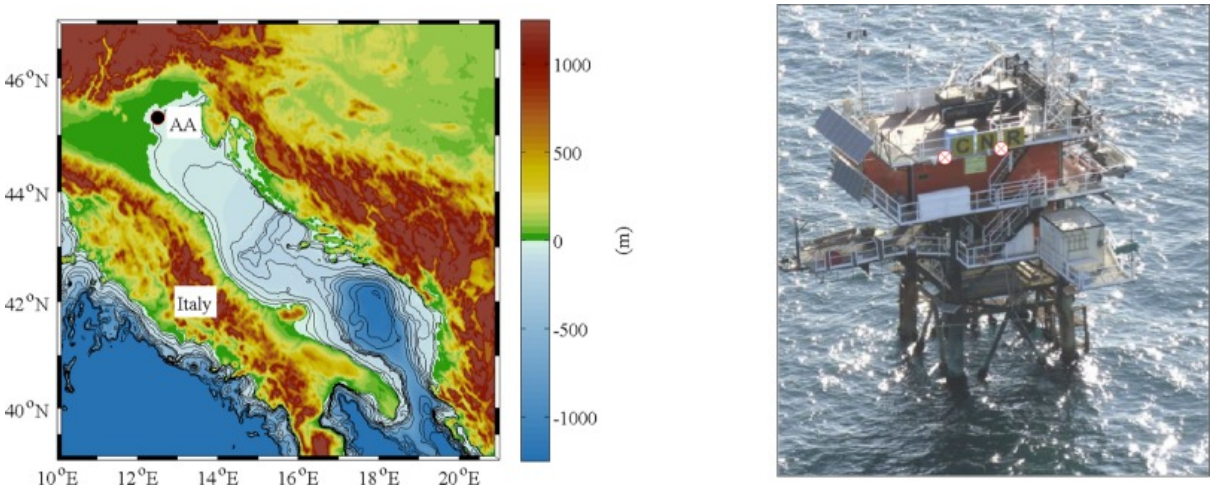

Fig. 3. (left panel) The Adriatic Sea (northern Mediterranean Sea) bathymetry and the surrounding orography. The black-red dot shows the position of the ‘‘Acqua Alta’’ oceanographic research platform (AA), which is situated 15 km off the Venetian littoral in (on average) 17 m deep water. (right panel) The platform structure and position of the stereo-camera system (white-red markers on the platform's roof). (For interpretation of the references to colour in this figure legend, the reader is referred to the web version of this article.)

The stereo-camera rig was based upon a Wave Acquisition Stereo System (WASS; Benetazzo, 2006, Benetazzo et al., 2012), which provides a time-sequence of 3D wave fields (see for example the sea surface elevation map shown in Fig. 4). The sea surface region framed by the stereo-camera system has area A of about 2900 m^2, and during the experiment (starting at 0940 UTC on 10 March 2014), WASS operated for a duration $D = 1798$ s. The WASS accuracy along the vertical direction is estimated about 3 cm (see Appendix B). For additional details on data processing and statistics, the reader is referred to Benetazzo et al. (2015).

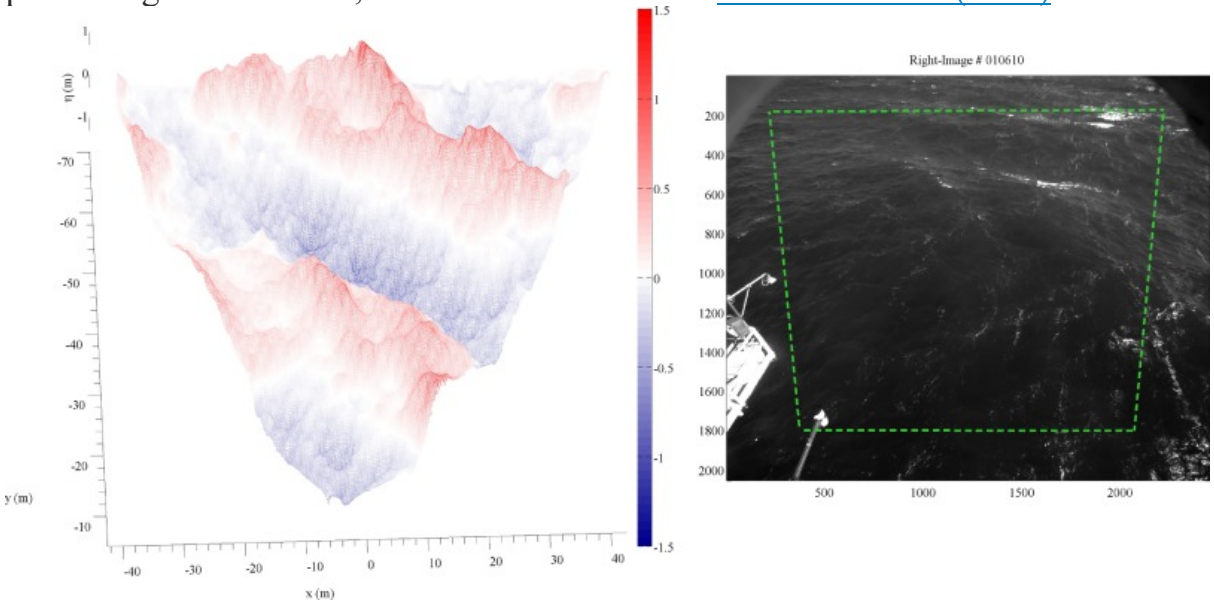

Fig. 4. (left panel) Example of 3D wave field retrieved by WASS, and (right panel) right stereo-camera image with highlighted (dashed green lines) the surface area used for stereo-matching. (For interpretation of the references to colour in this figure legend, the reader is referred to the web version of this article.)

Using the acquired sequence of 3D wave data, the frequency–direction wave spectrum $S(\omega, \theta)$ was estimated using the extended maximum entropy method (EMEP; Hashimoto et al., 1994); the $S(\omega, \theta)$ spectrum (shown in Fig. 5) was resolved with 180 equally spaced directions and 1024 equally distributed frequencies from 0.05 Hz to 2.00 Hz, the latter being also the cut-off frequency used to low-pass filter the data. Over the entire space-time sample, the significant wave height is $H_s = 4\sigma = 1.34$ m (where $\sigma = 0.334$ m is the standard deviation of η), the spectral mean zero-crossing period is $T_{m02} = 3.6$ s, the peak period is $T_p = 5.4$ s, and the mean direction of wave propagation $\theta_m = 248$ °N. The spectral width is $\nu = 0.50$. The sea state corresponds to a short-crested and mature wind sea with wave age $U_{10} / c_p = 1.31$, where $U_{10} = 11$ m/s is the wind speed at 10-m height measured during the experiment, and c_p is the linear wave phase speed corresponding to T_p. The one-sided width (directional spreading; Holthuijsen, 2008) of the omni-frequency directional distribution is 23°, which was computed between ± 90° the mean direction θ_m to limit the influence of noise. An estimate of the mean wave steepness μ was derived from the moments of the wave spectrum in accordance to Eq. (28) and results $\mu = 0.06$. The significant steepness that we define as $H_s k_p / 2$ (Adcock et al., 2015) is 0.09, where k_p is the wavenumber corresponding to T_p computed using the linear dispersion relation. The minimum value of the autocovariance function $\psi 1^*$ was derived from $S(\omega)$ and it is equal to −0.67.

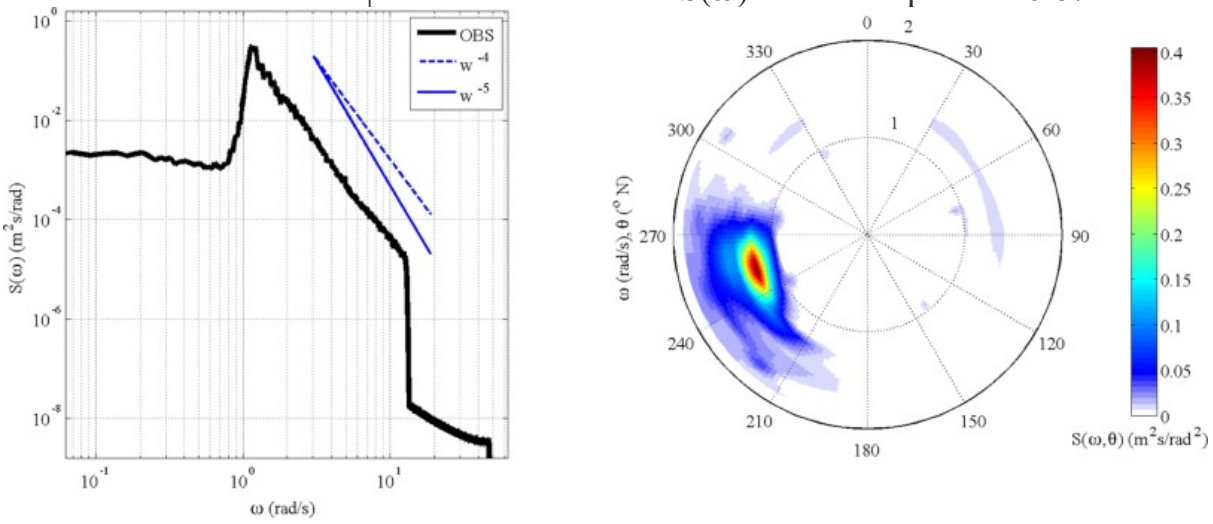

Fig. 5. - (left panel) Omnidirectional angular frequency spectrum estimated using the stereo wave data (OBS). The blue dashed and solid lines are reference spectral slopes

proportional to ω^{-4} and ω^{-5}, respectively. (right panel) Observed frequency–direction spectrum. (For interpretation of the references to colour in this figure legend, the reader is referred to the web version of this article.)

3.2. Space-time maxima

Following the procedure described in Benetazzo et al. (2015), the sea surface elevation 3D fields were analyzed to isolate the largest ST wave groups evolving within the region shown in Fig. 4. The analysis of grouping properties using remote sensors (e.g., Nieto Borge et al., 2013) or fully-nonlinear simulations (Sanina et al., 2016) has been typically conducted using ad-hoc techniques to detect coherent 3D groups. In this study, we have followed a somewhat simplified approach, in which wave groups were visualized within the 3D fields and then grabbed at the positions (x_i, y_i) where groups were supposed to be close to the apex of their development. Afterwards, only groups whose local maximum crest height exceeded the rogue wave threshold $1.25H_s$ were retained. In doing so, 23 spatial locations have been selected, and time records $\eta(x_i,y_i,t)$ extracted from the ST sample at the corresponding positions (x_i, y_i). Within each record, we selected the wave (labeled as Bi, with i = 1 to 23) with maximum crest height $\eta_{Bim} = \max\{\eta(x_i,y_i,t)\}$, which was referred to as a realization of the ST maximum elevation.

The individual and mean temporal profiles nearby the crests η_{Bim} are shown in Fig. 6, the surface elevation being normalized by H_s, and time by T_p. It is noteworthy that the general shape of the largest waves is regular: indeed profiles do not display positive minima, and the sea surface elevations are narrowly distributed around the highest crests (where the confidence in estimate of the mean is maximum). Notwithstanding, scattering of sea surface elevations occurs around the mean profile, and troughs preceding and following the extreme crests are highly dispersed both in amplitude and timing (even though the mean profile is rather symmetric, as we shall discuss in Section 4). The average zero-crossing period of the largest waves of the records is 4.7 s (smaller than T_p, consistently with the QD theory results), with a standard deviation of 0.4 s, and at the troughs of the mean profile the confidence is twice as larger as that at the crest. For comparison, Fig. 6 shows also the profile of the rogue wave recorded at the Draupner platform on 01 January 1995 (Adcock et al., 2011, Cavaleri et al., 2017, Fedele et al., 2016, Haver, 2004, Magnusson and Donelan, 2013); it is clear that all these “particularly high

crests" have, once normalized, very similar temporal profile. This strongly suggests that the Draupner wave was not so exceptional after all, simply reproducing on a larger scale what should be expected in those conditions as the highest crest of a dynamical space-time wave group passing close to the platform.

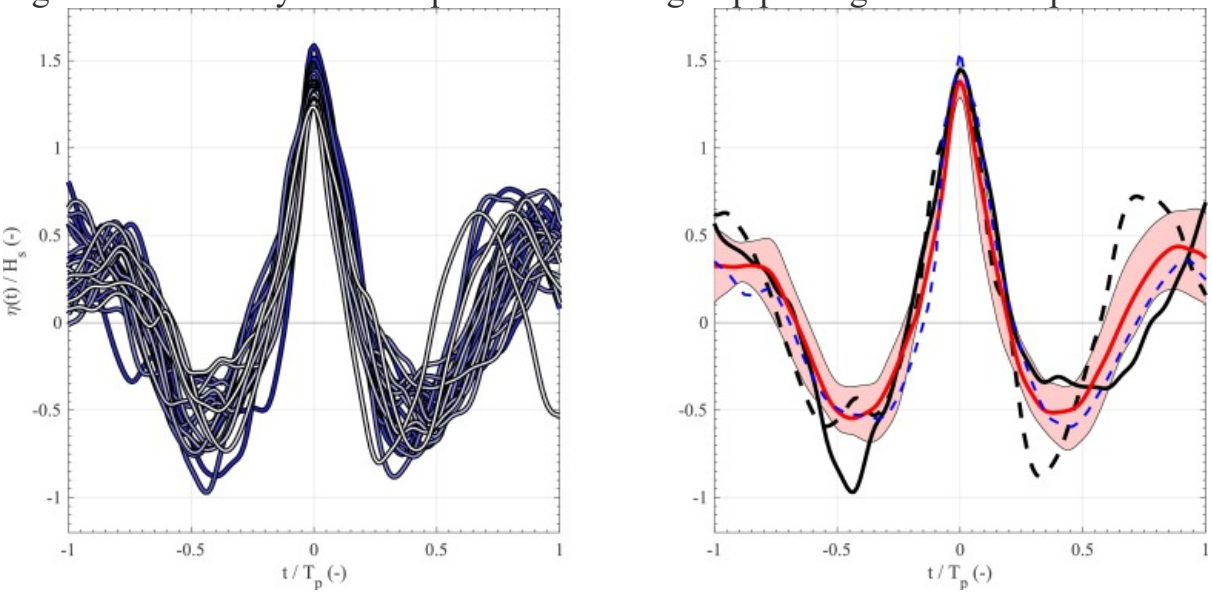

Fig. 6. Time series of the normalized profiles of the rogue waves Bi around the maximum crest heights η_{Bim}, versus the normalized time t / T_p. (left panel) Individual temporal profiles. (right panel) Mean profile (red) and its confidence band (red-shaded area, computed as the standard deviation of the elevations around the mean profile). Black curves show profiles of waves with maximum trough depth following the maximum crest (dashed line) and preceding the maximum crest (solid line). The dashed blue curve shows the Draupner rogue wave profile. For graphical purposes, maximum crest heights are imposed occurring at $t = 0$. (For interpretation of the references to colour in this figure legend, the reader is referred to the web version of this article.)

Summary statistics of the rogue waves Bi is shown in Table 1: the mean crest height is $\bar{\eta}_{Bm} = E\{\eta_{Bim}\} = 1.38H_s$, up to a maximum elevation of $1.59H_s$, and the mean maximum crest-to-trough wave height is $\bar{H}_{Bm} = E\{H_{Bim}\} = 2.08H_s$, with H_{Bim} ranging between $1.79H_s$ and $2.42H_s$.

Table 1. Statistics of the rogue waves Bi: crest height (η_{Bim}) and crest-to-trough height (H_{Bim}). Mean value (E{}), maximum value (max), minimum value (min), and standard deviation (*std*) of the variables are displayed.

Variable	**E{}**	**max**	**min**	***std***
$\boldsymbol{\eta_{Bim} / H_s}$	1.38	1.59	1.25	0.09
$\boldsymbol{H_{Bim} / H_s}$	2.08	2.42	1.79	0.16

3.3. Time (one-point) maxima

The crest and wave heights of the 23 waves Bi are compared with the maximum wave parameters derived from the ST wave field with no conditioning about the selection of the sea surface points (x_i, y_i). In doing so, we have resampled the data by randomly choosing 23 locations (x_p, y_p) on the *xy*-plane of Fig. 4. Time records at positions (x_p, y_p) have been processed with a zero-crossing analysis, and out of the 23 values we have retained the mean values (indicated by an overbar) of the quantities: maximum crest height ($\bar{\eta}_{pcm}$), crest-to-trough height of the wave with maximum crest height ($\bar{H}_{pcm}$), and maximum crest-to-trough height ($\bar{H}_{pm}$). We have then repeated 10^5 times the random sampling to derive a distribution of mean wave parameters (Fig. 7 and Table 2).

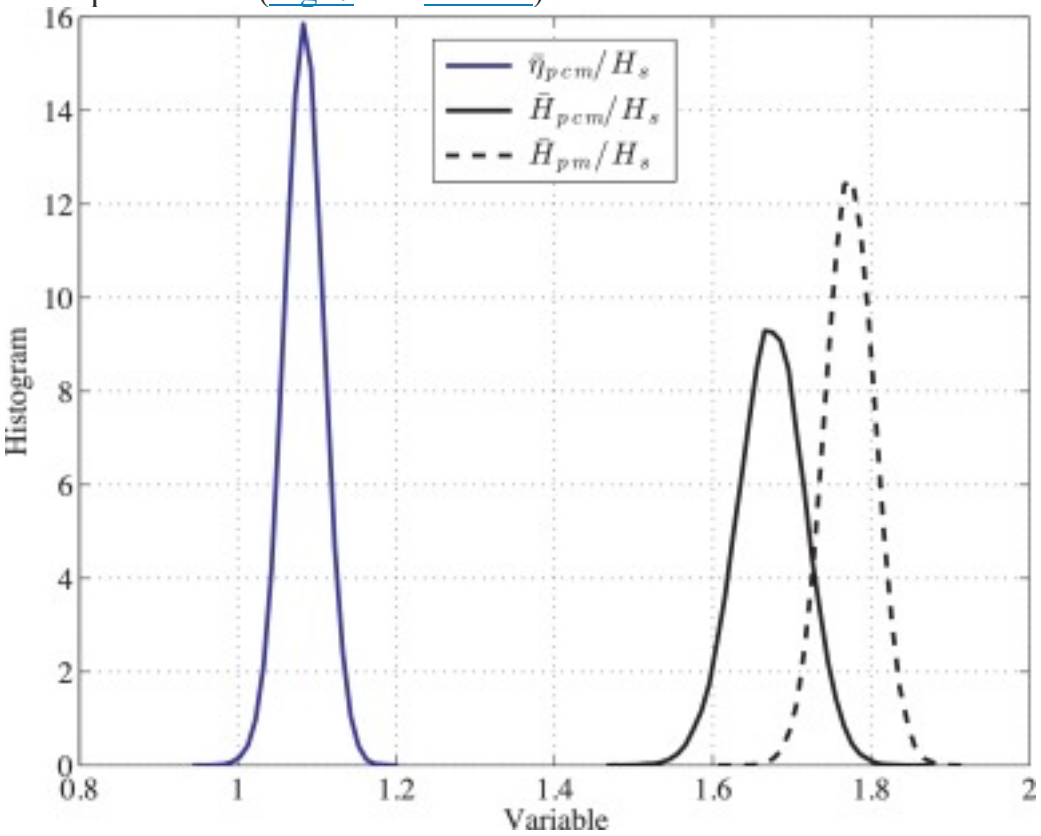

Fig. 7. Histogram of the one-point mean maximum crest height ($\bar{\eta}_{cpm}$ / H_s), associated crest-to-trough wave height ($\bar{H}_{pcm}$ / H_s), and maximum crest-to-trough wave height ($\bar{H}_{pm}$ / H_s). The sample space is the set of 10^5 randomly chosen realizations of 23 wave maxima on the *xy*-plane of Fig. 4.

Table 2. Statistics (over 10^5 randomly chosen realizations of 23 wave maxima on the *xy*-plane of Fig. 4) of the one-point mean maximum crest height ($\bar{\eta}_{pcm}$), mean crest-to-trough height ($\bar{H}_{pcm}$) of the waves with maximum crest, and mean maximum crest-to-trough height ($\bar{H}_{pm}$). Mean value (E{}), maximum value (max), minimum value (min), and standard deviation (*std*) of the variables are displayed.

Variable	E{}	max	min	*std*
$\bar{H}pm / H_s$	1.77	1.90	1.62	0.03
$\bar{H}pcm / H_s$	1.67	1.86	1.46	0.04
$\bar{\eta}pcm / H_s$	1.08	1.19	0.95	0.03

The average value of the mean quantities are $E\{\bar{\eta}pcm\} = 1.08H_s$, $E\{\bar{H}pcm\} = 1.67H_s$, and $E\{\bar{H}pm\} = 1.77H_s$, all with similar (and small) variability (*std* in Table 2) around the mean (indeed distributions shown in Fig. 7 are rather narrow). At most, the maximum average crest height is $\max\{\bar{\eta}pcm\} = 1.19H_s$, largely smaller than $\bar{\eta}Bm = 1.38H_s$, as well as $\max\{\bar{H}pcm\} = 1.86H_s < \bar{H}Bm = 2.08H_s$. These results clearly indicate that, for short-crested waves, the largest wave elevations occur at specific positions of the sea surface, and without a conditioning on the selection of time series it is unlikely to gather (on average) very large sea surface elevations. This constraint imposed on the observational strategy has consequences for the measurement of rogue waves.

4. Results

4.1. Comparison between space-time and time extreme waves

In this section outputs of theoretical models used to predict extreme waves' parameters will be assessed with observations. Firstly, we compare (Fig. 8) the histogram of the observed ST maxima η_{Bim} with the Gumbel-like probability density function (pdf) approximating the linear P_{1STm} (see Appendix A) and nonlinear P_{2STm} distribution functions. As already pointed out by Benetazzo et al. (2015), despite the limited number of observational data, there is close agreement between the empirical and the theoretical pdf of nonlinear ST extremes. As a result, assuming extreme elevations η_{Bim} relative to a duration $D = 1798$ s and a sea surface region with sides $X = Y = 11.2$ m (corresponding to the side of a square with area $A / 23$), the expected value of the nonlinear ST maximum crest height is $\bar{\eta}2STm=1.37Hs(\sigma m2=0.10Hs)$, which agrees favorably with the observed mean maximum $\bar{\eta}Bm$. Assuming a Gaussian wave field, the theoretical pdf is shifted towards smaller elevations, in a way that the expected value of the linear ST maximum crest is height $\bar{\eta}1STm=1.19Hs(\sigma m1=0.08Hs)$, about 13% smaller than $\bar{\eta}2STm$.

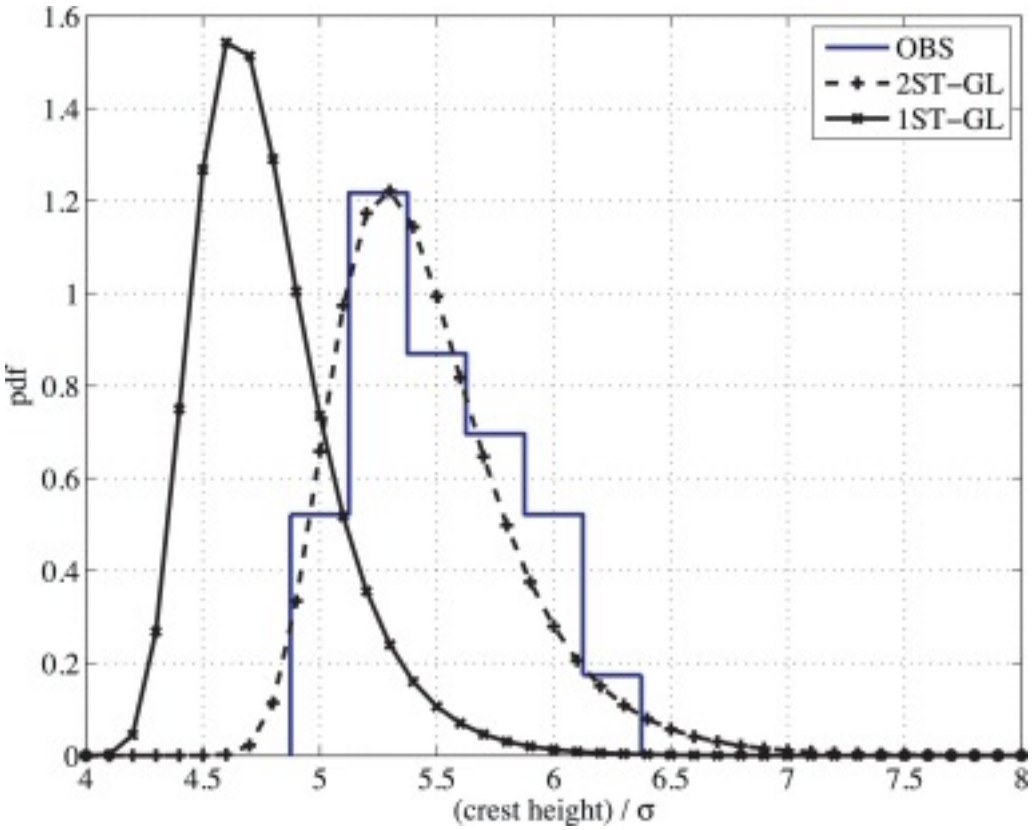

Fig. 8. Distribution of ST extreme sea surface elevations. The empirical histogram (OBS) is calculated using the maximum crest heights η_{Bim} of the rogue waves Bi. The empirical function is compared with the Gumbel approximation of the second-order nonlinear pdf (2ST-GL) and linear pdf (1ST-GL) of ST extreme elevations.

Secondly, the extreme wave parameters derived from one-point wave records (Section 3.3) are compared with the expectations of theoretical model developed for the prediction of maxima in time series of sea surface elevations. In this respect, the expected value of the maximum linear wave height (H_{1Tm}) in a time-sequence of N waves is computed as the integral of the probability of exceedance as follows(34)H¯1Tm=∫0∞Pr{H1Tm>H}dH=∫0∞1−{1−exp[−41−ψ1*(HHs)2]}NdHwhere we have assumed wave heights H in a time record distributed according to the Boccotti's asymptotic formula (Boccotti, 2000), which holds for linear waves and accounts for the spectral bandwidth (expressed by the parameter ψ1*).
In our case, the average number of waves in the record is $N = D / T_{m02} = 1798 / 3.6 = 499$, and the expected maximum wave height is $H¯1Tm= 1.68H_s$, which underpredicts of about 5% (mainly due to nonlinear effects; see Section 4.2) the observed value $E\{H¯pm\} = 1.77H_s$. Moreover, assuming crest heights in a wave record distributed according to the second-order nonlinear Tayfun (1980) model,

we have computed an expected time extreme crest height of $\bar{\eta}_{2Tm} = 1.03H_s$, about 5% smaller than the observed mean $E\{\bar{\eta}_{pcm}\}$.
Additionally ST and time extreme wave parameters derived in Sections 3.2 and 3.3, respectively, are inter-compared to assess the relationship, if any, between maximum crest heights and maximum crest-to-trough wave heights. For the case of the 23 waves Bi the ratio $r_{ST} = E\{H_{Bim} / \eta_{Bim}\} = 1.51$ is close to the ratio derived using one-point time extremes, $r_T = E\{\bar{H}_{pcm}/ \bar{\eta}_{pcm}\} = 1.54$, confirming the presence of a similarity law (trough the autocovariance function) between maximum crest and wave heights at different scales. This provides an aspect in which maximum wave events (whether rogue or not) do not differ, as it has been already noticed by Christou and Ewans (2014). The two ratios r_{ST} and r_T are overestimated by the prediction of the linear QD model that would provide the value $(1 - \psi 1^*) = 1.67$, but they are well determined by the nonlinear extension of the QD theory, which, for a linear crest height of $1.25H_s$ (as in Fig. 2) predicts a ratio equal to 1.55. Also, for point-like wave observations the ratio $r_{pH} = E\{\bar{H}_{pm}\} / E\{\bar{H}_{pcm}\} = 1.06$ is larger than 1, and it is explicitly computable using Eq. (17), which, for $\psi 1^* = -0.67$, provides $r_H = 1.09$.
In this respect, Fedele (2015) guessed the presence of a scaling law between the ratio $r_{2m} = \bar{\eta}_{2STm}/ \bar{\eta}_{2Tm}$and the normalized sea surface area XY used to compute the ST extremes. Focusing on the data used in this paper, Fig. 9 shows the distribution of r_{2m} as a function of the normalized area $r_A = (XY) / (L_x L_y)$, where L_x and L_y are the mean zero-crossing wavelength and the mean wave crest length, respectively. We note a strong dependence of r_{2m} on r_A, confirming what shown by Fedele et al., (2013) and Barbariol et al., (2015) using observational and numerical data, respectively. As a preliminary attempt, observational data has been least-square fitted with a power law of the type(35)r2m=a(rA)b+1which, passing through the origin, guarantees that $\bar{\eta}_{2STm} = \bar{\eta}_{2Tm}$ when the spatial area collapses to a single point (i.e. $XY = 0$). The empirical coefficients from the present fit are $a = 0.38$, $b = 0.12$, which provides a good fitting to the data (root-mean-square error is $\sim 10^{-2}$). However, as the extreme $\bar{\eta}_{2STm}$ is also function of D and T_m, which have been excluded by the law (35), we have verified (not shown here) a dependence of coefficients a and b on the ratio D / T_m. This functional dependence, as well as the relation of r_{2m} to other parameters as the wave steepness, should be further investigated.

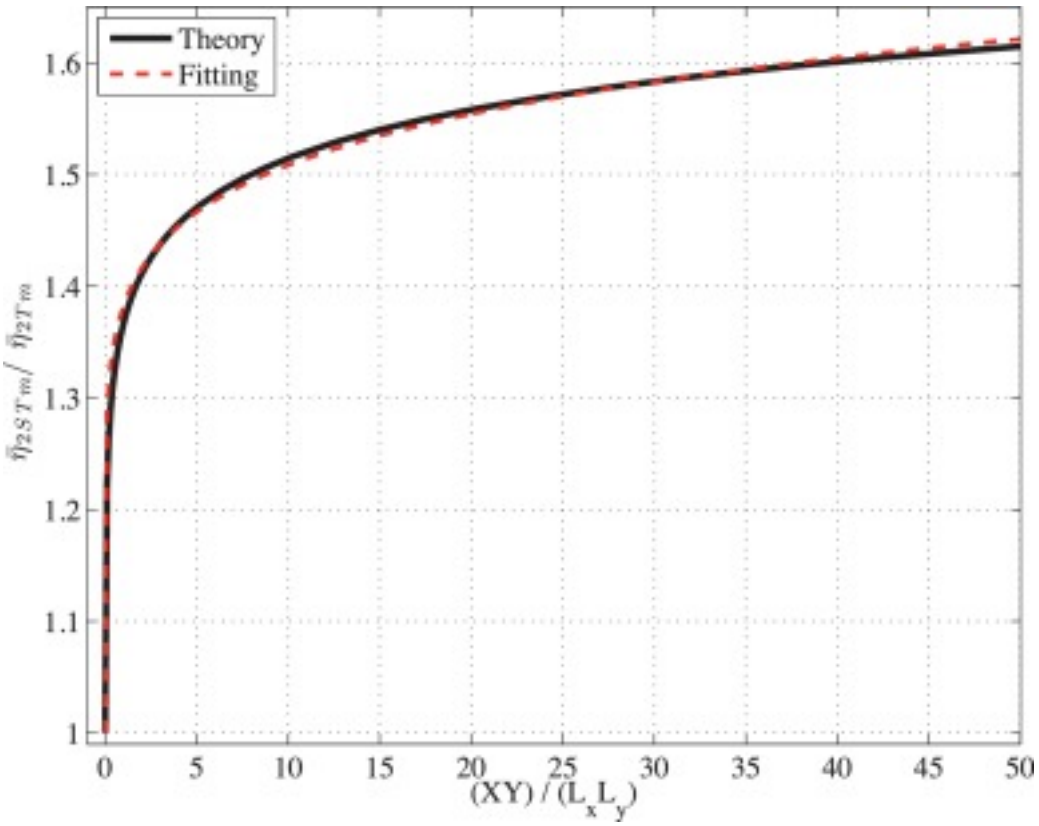

Fig. 9. Observation of space-time and time extreme crest heights. The black solid line shows the ratio between the second-order nonlinear ST ($\eta^{-}2STm$) and time extremes ($\eta^{-}2Tm$) as a function of the normalized sea surface area $(XY) / (L_xL_y)$. The average number of waves in the time record is 499. A power-law type fitting curve is shown as dashed red line. (For interpretation of the references to colour in this figure legend, the reader is referred to the web version of this article.)

4.2. Comparison between theoretical and empirical wave profiles and heights

In this section we shall examine how well temporal profiles and wave heights of the rogue waves extracted from the ST sample (Section 3.2) agree with the results of the QD and ST models. Assuming dominant the second-order nonlinearities, in the following, we neglect the differences, in the order of $O(\mu^2)$, between first- and second-order spectral densities. Therefore we derive the ST autocovariance function $\psi_1(\boldsymbol{X}, \tau)$ from the observed directional spectrum $S(\omega, \theta)$, and the temporal functions $\psi_1(\tau)$ and $\lambda(\tau)$ from the omnidirectional spectra $S(\omega)$ and $S(k)$, respectively. The minimum of the autocovariance function $\psi_1(\tau)$ occurs at time $\tau^* = 2.30$ s, close to mean half-cycle period (2.35 s) of the waves Bi.

4.2.1. Predictions of the QD model

Aiming at predicting the shape of the rogue waves Bi we have firstly used the QD model to estimate the mean linear profile η¯1Bi(τ) of the maximum wave of each record. To this end, the linear component (η_{1Bim}) of the observed maximum crest heights (η_{Bim}) was derived using the Tayfun quadratic Eq. (27) as follows(36)η1Bim=σ−1+1+2μηBim/σμ

The expected value of the linear crest height is E{η_{1Bim}} = 1.21H_s, which is in very good agreement with the prediction η¯1STm = 1.19H_s of the Gaussian ST extreme model. For each wave Bi the mean linear profile (hereinafter 1QD) around η_{1Bim} is, according to (6), given by(37)η¯1Bi(τ)=η1Bimψ1(τ)σ2which is shown in Fig. 10 for 4 (namely B01, B07, B20, B22) out of the 23 waves. It can be seen that the linear profiles η¯1Bi(τ), apart from the expected underestimation of the maximum crest height, predict crests less steep and troughs shallower than those of the observed waves. The similarity between the observed and the linear waves is measured by the cross-correlation coefficient (*CC*) between the profiles within the time interval (-τ*, +τ*). The value of *CC* (Table 3) is on average 0.95, at most *CC* = 0.99 for the record B20, and at least *CC* = 0.86 for the record B22. The latter (see bottom-right panel of Fig. 10), indeed, displays elevations around the crest that significantly deviate from the theoretical wave group shape at ***X*** = (0, 0). The ratio ρ between standard deviations of observed and theoretical linear profiles within the time interval (-τ*, +τ*) is 0.87 on average, that is, the variance of the theoretical profile around the maximum crest is generally larger than the variance of the observations.

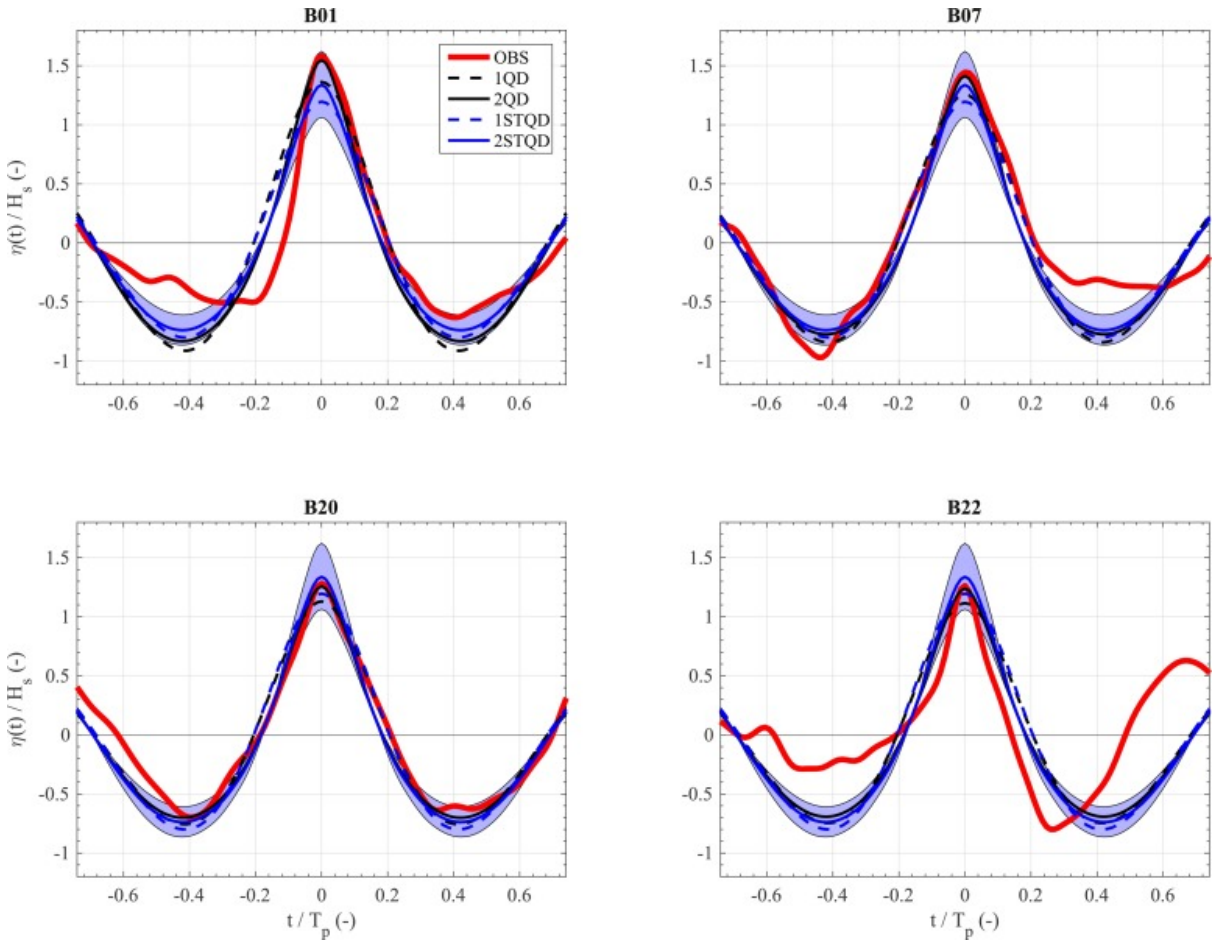

Fig. 10. Time series of the normalized profiles of the rogue waves Bi around the maximum crest heights η_{Bim}, versus the normalized time t / T_p. OBS: observed wave profile. Theorethical profiles: 1QD, linear QD model; 2QD, second-order nonlinear QD model; 1STQD, linear ST prediction and QD model; 2STQD, second-order nonlinear ST prediction and QD model. The blue-shaded area represents the 99% confidence interval of 2STQD. (top-left) Wave B01 with maximum crest height. (top-right) Wave B07 with maximum crest-to-trough wave height. (bottom-left) Wave B20 with maximum *CC* between OBS and 2STQD. (bottom-right) Wave B22 with minimum *CC* between OBS and 2STQD. In Figure, the time lag τ is indicated with the time axis t, and $t_0 = 0$. (For interpretation of the references to colour in this figure legend, the reader is referred to the web version of this article.)

Table 3. Statistical parameters of observed and theoretical extreme wave shapes around the maximum crest height within the time interval $(-\tau^*, +\tau^*) = (-2.3\text{ s}, 2.3\text{ s})$. OBS: observed waves. Theorethical profiles: 1QD: linear QD model; 2QD: second-order nonlinear QD model; 1STQD: linear ST prediction and QD model; 2STQD: second-order nonlinear ST prediction and QD model. Variables: E{H}: mean wave height; E{CC}: mean *CC* between observed and theoretical profiles; E{ρ}: mean ratio between the standard deviations of observed and theoretical profiles.

Variable	OBS	1QD	2QD	1STQD	2STQD
E{*CC*}	–	0.95	0.97	0.95	0.97
E{*ρ*}	–	0.87	0.89	0.88	0.89
E{*H*} / *H*ₛ	2.08	2.01	2.10	2.00	2.08

For each wave Bi, the theoretical profile of the second-order nonlinear elevation is, according to (10), evaluated as(38)η¯2Bi(τ)=η1Bimψ1(τ)σ2+16η1Bim2λ(τ)σ4=η¯1Bi(τ)+16η1Bim2λ(τ)σ4and it is displayed in Fig. 10 as 2QD. As we can infer from Table 3 the nonlinear formulation improves the performances of the predictions based on the QD model. Results shown in Fig. 10 deserve some considerations that can explain the differences between observed and theoretical profiles. Firstly, we have allowed a comparison between an expectation (1QD and 2QD) and a single realization (OBS) of a stochastic process. Strictly speaking, for the sake of assessment, we would need a set of independent realizations of waves with given crest height, from which inferring an empirical mean profile. Secondly, the QD model that predicts the temporal profile of waves with large crests assumes that the wave crest is at its maximum elevation (and thus at the wave group center $\boldsymbol{x}_0$). This condition, most likely, was not satisfied by all waves. Indeed, the limited spatial extension of the stereo-camera field of view restricted the possibilities to collect the complete ST dynamics of the wave groups. Therefore, although crest heights were indeed local maximum elevations of the groups, the positions (x_i, y_i) of the waves Bi were close to, but not exactly at the envelope center. Thus, for comparison, we should consider the ST group at a position (different for each wave) displaced from the unknown position $\boldsymbol{x}_0$. The effect of this critical task is illustrated, for example, in Fig. 11, where three temporal profiles of the ST autocovariance function are displayed: the profile at the focusing point $\boldsymbol{x}_0$ (where $\boldsymbol{X} = 0$), which corresponds to $\psi_1(\tau)/\sigma^2$, and two profiles taken at positions displaced from $\boldsymbol{x}_0$. We note that the latter have smaller crest height and an asymmetric shape around the maximum elevation (see also for comparison the observed profiles with maximum trough depth shown in Fig. 6). The question remains, for any wave record, as to what temporal transect of the ST autocovariance must be used to infer statistical properties of the one-point observation of maxima.

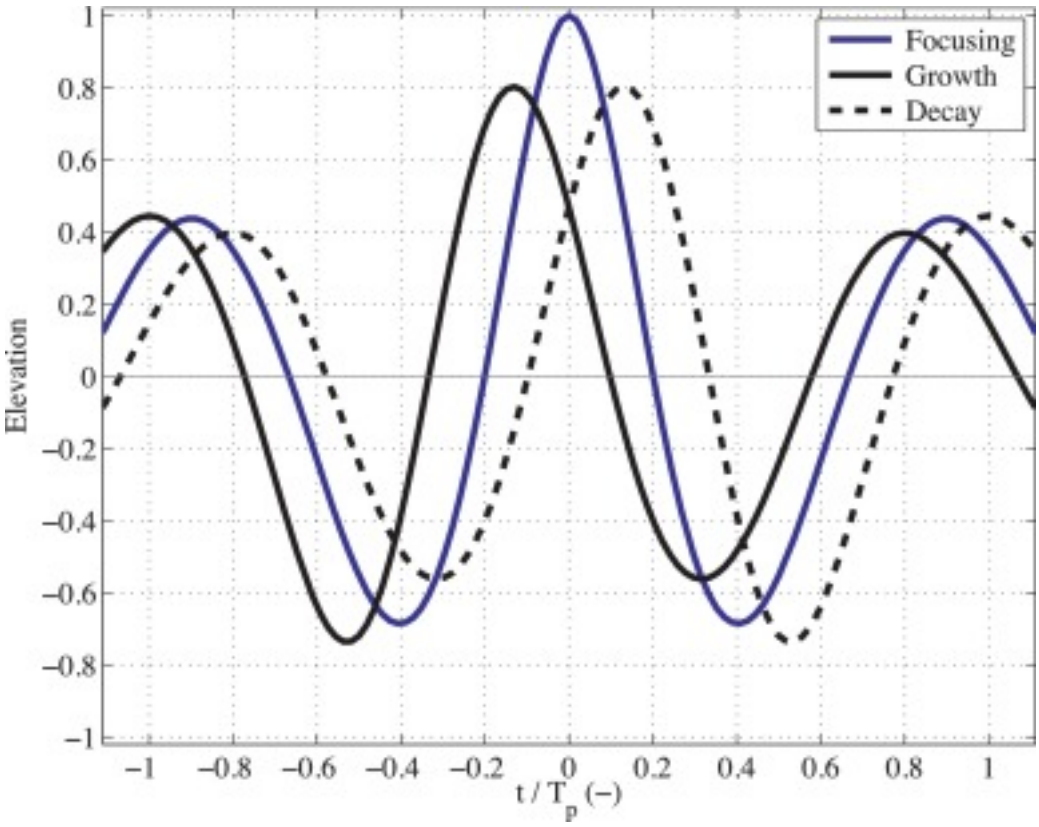

Fig. 11. Time series of the normalized temporal profile of the linear ST group at different spatial positions: i) focusing point, where the group exhibits its maximum crest elevation (blue line); ii) growth stage (solid black line); iii) decay stage (dashed black line). In Figure, the time lag τ is indicated with the time axis t, which is scaled with T_p, and $t_0 = 0$. (For interpretation of the references to colour in this figure legend, the reader is referred to the web version of this article.)

Observing the theoretical profiles in Fig. 11 we recognize that, changing the point of observation of the ST group, whilst the crest height shrinks (of about 20%) while leaving the envelope center, the maximum wave height decreases to a lesser extent (about 8%). We have also seen in Section 2.1.3 that the wave height is slightly influenced by the second-order nonlinearities. Both of these conditions could be the reason why the mean value of the linear crest-to-trough height of the waves Bi given by(39)H¯1QD=E{η1Bim}(1−ψ1*)and equaling 2.01H_s well agrees (difference of about 3%) with H¯Bm (OBS in Table 3). As expected, however, inclusion of nonlinearities improve the performance of the QD model (in Eq. (19) the coefficient $\beta = 1.5*10^{-5}$ m^{-1}), and it is relevant that the mean maximum nonlinear wave height given by(40)H¯2QD=E{η1Bim(1−ψ1*)+λ(0)−λ*6σ4η1Bim2}is very close (H¯2QD = 2.10H_s in Table 3) to H¯Bm (difference of 1%).

These results, albeit assessed on a single dataset, indicate that linear and nonlinear versions of the QD model can be successfully used to estimate the mean wave height of ST extreme waves in a time record. A shortcoming of this theory is that the resulting model cannot be regarded as a complete predictive model, as it relies on the observed crest height (and its linear part). This limitation will be discussed in the next section, where the predictions of the ST extreme model will be used to scale the theoretical profiles of wave groups.

4.2.2. Predictions of the combined QD and ST models

The results presented so far have shown that scaling the time-dependent wave profiles with the autocovariance function allows the prediction of extreme waves heights in terms of spectral integral quantities. The practical application of QD is limited by the assumption that the sea surface maximum elevation is known *a priori*, which is not always doable in practice. However, we have seen that a high local maximum is, with a very high probability, also the crest height of a wave within a specific 3D wave group, and that the expected value of the highest wave crests is well approximated by the prediction of the second-order nonlinear ST extreme model. This would suggest the use of the QD theory adopting, as scale factor, the ST extreme model predictions.

Along this line, we thus stop trying to reproduce each single wave profile Bi, as we have done in the previous section, but rather we attain a mean time-dependent profile that is compared with the waves Bi. In this respect, linear (hereinafter 1STQD) and second-order nonlinear (hereinafter 2STQD) sea surface profiles around the maximum crest are scaled with $\eta^{-}1STm$ and they are respectively given by(41)$\eta^{-}1ST(\tau)=\eta^{-}1STm\psi1(\tau)\sigma2(42)\eta^{-}2ST(\tau)=\eta^{-}1STm\psi1(\tau)\sigma2+16\eta^{-}1STm2\lambda(\tau)\sigma4=\eta^{-}1ST(\tau)+16\eta^{-}1STm2\lambda(\tau)\sigma4$

The temporal profiles $\eta^{-}1ST$ and $\eta^{-}2ST$ are compared (Fig. 10) with the observations and their statistical performances are presented in Table 3. The linear profile $\eta^{-}1STh$as statistics very similar to those of 1QD, as we have seen that $\eta^{-}1STm \approx \eta^{-}Bm$. A better performance is provided by 2STQD that predicts the mean maximum wave height equal to $H^{-}Bm$. Being $CC = 0.97$ on average, the OBS and 2STQD temporal profiles have a very high correlation (at most $CC = 0.99$ for B20 in Fig. 10), despite the ratio ρ of the standard deviations is still smaller than 1, as a consequence that the theoretical profiles are generally more rounded around the mean level than the observations.

5. Conclusions

In this study we have investigated the shape and height of extreme waves collected within a space-time sample of sea surface elevations. The sample has been analyzed to gather 3D moving wave groups where and when they were close to the apex of their development and consequently they exhibited largest elevations. Wave time records at the 2D position of ST maxima have been extracted from the sample and they have become main object of our study. In particular, we have examined the maximum crest height (always exceeding the rogue wave threshold $1.25H_s$), the maximum wave height, the height of the wave with maximum crest height, and the temporal profile of the extreme wave of each record. Observations have been compared, on the one hand, with results of space-time and time stochastic model for nonlinear wave extremes, and, on the other hand, with the predictions of the linear and nonlinear Quasi-Determinism model for the shape of very high waves.

Moreover, results of ST extreme (via Euler Characteristic approach) and QD models have been coupled in a common framework to estimate, from a given wave energy directional spectrum, temporal profiles and heights of maximum waves during a sea state. This has implications for numerical predictions of extreme wave profiles and heights. In this respect, the computations of maximum crest and wave heights as formulated in this study are implemented as new outputs of the numerical wave model WAVEWATCH III® version 5.16 (WW3DG 2016, Barbariol et al., 2017).

Main results of the study can be summarized as follows:

•Compared to observations, the QD model predicts favorably the average height of waves with maximum crest height. The most likely reason for this is that, as the central wave of the group runs throughout the envelope center, the crest-to-trough height of the maximum wave changes, but not too much (differences are generally smaller than 10%). The second-order nonlinear extension of the QD model provides a better agreement, but differences between linear and nonlinear estimates are small (in the order of 2 to 3%).

•The height of waves with maximum crest height is smaller (of about 5 to 10%) than the maximum wave height in a wave record: this is a corollary of the QD theory, which is also able to determine the relationship between the two heights. Theoretical results have been confirmed by the observations.

•Care must be taken when comparing one-point observations of the profile of very large waves and predictions based on the autocovariance function (the core of the QD theory). In this study we have discussed reasons that can weaken a fair comparison. It is worth recalling that a comparison between observed and theoretical profiles is possible only if measurements are collected at the sea surface position where the maximum crest elevation is at the ST group center (i.e. the focusing point). For oceanic observations, this condition cannot be always satisfied neither verified, thus QD model for single wave profile estimation should be used carefully.
•We have analyzed the similarity between ST and time maximum wave parameters. We have verified that wave heights and crest heights relate at all scales in a similar behavior, which is well predicted by a second-order nonlinear extension of the QD model. Moreover, in search of a universal law connecting ST and time extremes, we have preliminarily explored how the ratio between the two extremes does change as a function of the sea surface area used to compute the ST extreme probability.
•Even though it is not an original result that maximum elevations (even belonging to rogue waves) of 3D wave groups are well predicted by stochastic models for ST extremes, we have seen that for short-crested waves it is unlikely to gather these maxima unless one would be able to observe the 3D groups at the apex of their development. In this condition, we have seen that ST extreme and QD model results may be coupled in a predictive model for maximum wave heights within a sea state with specified wave energy spectrum. Indeed, all variables used to predict the temporal wave profiles $\eta^{-}1ST(\tau)$ and $\eta^{-}2ST(\tau)$ are derived from integral quantities of the directional wave spectrum (see also Appendix C).

Acknowledgements

The authors gratefully acknowledge the funding from the Flagship Project RITMARE — The Italian Research for the Sea — coordinated by the Italian National Research Council and funded by the Italian Ministry of Education, University and Research within the National Research Program 2011–2015. We are thankful to Dr. Mauro Bastianini (CNR-ISMAR) for assistance on the "Acqua Alta" platform (http://www.ismar.cnr.it/infrastructures/piattaforma-acqua-alta?set_language=en&cl=en), to Dr. Luigi Cavaleri (CNR-ISMAR) for useful

comments and suggestions, and to anonymous reviewers whose comments and questions have improved the final paper. The code for stereo reconstruction of 3D wave fields is available as free software at http://www.dais.unive.it/wass/.

Appendix A. The EC model for ST extreme of Gaussian wave fields

The *EC* approach (Adler, 2000, Adler, 1981) was introduced in the field of oceanic waves by Baxevani and Rychlik (2006), and afterwards extended to include the complete ST structure of the covariance matrix Λ by Fedele (2012). Considering a Gaussian sea state over a ST domain (dimension $N = 3$) the matrix Λ becomes(A.1)Λ=[E{η1xη1x}E{η1xη1y}E{η1xη1t}E{η1yη1x}E{η1yη1y}E{η1yη1t}E{η1tη1x}E{η1tη1y}E{η1tη1t}]where $\nabla\eta_1 = (\eta_{1x}, \eta_{1y}, \eta_{1t})$, and η_{1x}, η_{1y}, η_{1t} are the first-order derivative of η_1 with respect to the x-, y-, and t-coordinate, respectively. Using the random-phase/amplitude model results, the minors of the covariance matrix Λ can be determined from the moments m_{ijl} of the wave spectrum $S(\omega, \theta)$ defined as follows(A.2)mijl=∫∫kxikyjωlS(ω,θ)dωdθ.

Moments m_{ijl} with $i \neq 0$ and $j \neq 0$ depend on the orientation of the coordinate system and it should be a natural choice to select the x- and y-axis orientation in such a way that the variance of spatial derivatives along one axis (say x) is maximized (Baxevani and Rychlik, 2004). This condition is satisfied assuming the mean direction of wave propagation coincident with the x-axis, and it is used as reference direction in this study.

Using the spectral moments the determinant of Λ can be written as (Fedele, 2012)(A.3)detΛ=m200m020m002(1+2αxtαxyαyt−αxt2−αxy2−αyt2)where the following parameters(A.4)αxt=m101m200m002;αyt=m011m020m002;αxy=m110m200m020measure the "irregularity" of the sea state, as they equal the normalized cross-correlation coefficient between the components of the sea surface gradient. It is worth noting that while some moments m_{ijl} change with the orientation of the axes (Baxevani and Rychlik, 2004), the determinant of Λ, and consequently the ST extreme estimate, is unaffected by an axes rotation. With the selected axes, moments m_{200} m_{020} and m_{002} are associated with the mean zero-crossing period (T_{m02}), the mean zero-crossing wavelength (L_x) and the mean wave crest length (L_y) by the following(A.5)Tm02=2πm000m002;Lx=2πm000m200;Ly=2πm000m020where $m_{000} = \sigma^2$ is the variance of the ST field $\eta_1(x, y, t)$.

Using the definition of E{$EC(S_{U,z})$} and the approximation (25) the probability that the maximum sea surface elevation exceeds the linear threshold $z = z_1$ over the interior domain $\Omega \in \Re^3$ of U is given by (Fedele, 2012)(A.6)P3D=Pr{η1STm>z1|Ω}=N3[(z1σ)2−1]PR(z1)where $N_3 = 2\pi N_{3D}$, and N_{3D} approximates the average number of 3D waves within U and it is given by(A.7)N3D=XLxYLyDTm021+2αxtαxyαyt−αxt2−αxy2−αyt2and(A.8)PR(z1)=exp(−z122σ2)is the Rayleigh probability of exceedance for crest heights. In (A. 7) X and Y are the side lengths of the horizontal sea surface covered by U, and D is its duration. If we consider a portion of U spanning the boundary surfaces (i.e. XD, YD and XY in $\Re^2$) of U, the probability that the threshold is exceeded on these surfaces can be expressed as(A.9)P2D=Pr{η1STm>z1|XD,YD,XY}=N2z1σPR(z1)where $N_2 = 2\pi N_{2D}$, and N_{2D} approximates the average number of 2D waves on surfaces XD, YD and XY and it is given by (A.10)N2D=(XDLxTm021−αxt2+XYLxLy1−αxy2+YDLyTm021−αyt2)

For domains in $\Re^1$ (namely the edges X, Y and D of the region U) the probability of exceedance of the absolute maximum is expressed as(A.11)P1D=Pr{η1STm>z1|X,Y,D}=N1PR(z1)where $N_1 = N_{1D}$ approximates the average number of 1D waves as follows(A.12)N1D=XLx+YLy+DTm02

The final expression for P_{1STm} is obtained correcting P_{3D} with P_{2D} and P_{1D} to account for the possibility that the excursion set touches the boundary / edges of U (Worsley, 1996). The exceedance probability P_{1STm} is thus approximated for $z >> \sigma$ as follows (Fedele, 2012)(A.13)P1STm=Pr{η1STm>z1|U}={N3[(z1σ)2−1]+N2z1σ+N1}PR(z1)

The inclusion of the three probability functions into the general formula (A.13) was argued by Romolo and Arena (2015). However, the correction of the 3D term has been proved to be in fair agreement with experimental data (Fedele et al., 2013), and it becomes negligible as soon as the X and Y spatial dimensions of the region U become comparable or larger than the reference wave lengths L_x and L_y (Fedele, 2015).

The expected value (η^-1STm) of η_{1STm} is determined approximating the probability of extremes P_{1STm} with a Gumbel distribution (Fedele, 2012, Socquet-Juglard et al., 2005), which provides the following equation (Gumbel, 1958)(A.14)η¯1STm=E{η1STm}=σh¯1STm≈σ(h1+γα1)where $\gamma \approx 0.5772$ is the Euler-Mascheroni constant, α_1 is the intensity function (equal to the reciprocal of the scale parameter of the Gumbel distribution), and h_1 is the normalized most

probable (namely mode) linear extreme value, which is approximated as the largest positive solution of the following implicit equation
in h(A.15)(N3h2+N2h+N1)exp(−h22)=1
The intensity function α_1 is given by(A.16)α1=h1−2N3h1+N2N3h12+N2h1+N1such that the normalized mean maximum elevation h¯1STmis given by(A.17)h¯1STm=h1+γ(h1−2N3h1+N2N3h12+N2h1+N1)−1
The uncertainty of the estimate η¯1STm is defined as follows (Gumbel, 1958)(A.18)σ1m=σπ6α1=σπ6(h1−2N3h1+N2N3h12+N2h1+N1)−1in a way that the 99% confidence interval of the largest values distribution is bound by $\pm 3\sigma_{1m}$ around the mean value.

Appendix B. Accuracy of the stereo wave imaging system

In this Appendix we take a look at the errors associated with the stereo reconstruction of the 3D sea surface. Two principal sources of uncertainties can be expected in any stereo method: the uncertainty in the determination of the corresponding pixels (*matching error*) and the uncertainty in the recovery of 3D coordinates (*quantization error*). Indeed, when designing a stereo-camera system one must compromise to meet mainly the conflicting requirements of accurate 3D estimation and accurate image feature matching. In fact, as pointed out by Mironov et al., (2012), the major difference between stereo wave imaging and the classical problem of stereo reconstruction is in the fact that the water surface reflectance is not Lambertian. However, Benetazzo (2006) shown that the matching error is small for highly-textured water surfaces, and Jähne (1993) indicates that the matching error is small when the wave slope is much larger than the inclination of the stereo cameras optical axis. For installing the cameras, the geometry of the stereo rig was empirically tuned so that the interplay between the light vector, the point of view and the surface normal is similar for the two cameras. Thus, we assume that the disparity of each corresponding pixel is dominated by the spatial position of the 3D surface point and not by the rather complex water surface bidirectional reflectance distribution function.
To provide an accurate 3D reconstruction, care has to be taken when choosing the imaging system parameters, the principal being the camera cell size and pixel numbers, the focal length, the baseline, the camera reciprocal orientation, and the distance from the stereo-camera system to the scene of interest. Under general conditions, in order to keep small the range error due to quantization (hence to

provide high accuracy in the 3D reconstruction) the baseline-to-distance ratio must be large; however, accurate feature points matching requires that this ratio be small (Jähne, 1993, Rodriguez and Aggarwal, 1990). An optimal set-up must be found. Based on our experience on stereo wave imaging at the sea (Benetazzo, 2006, Benetazzo et al., 2016, 2015, 2012) the correspondence problem is negligible, in absence of sun glitters, setting stereo cameras with optical axes (almost) parallel in order to reduce as small as possible the angle between them, and letting the average baseline-to-distance as small as possible (around 0.10, much smaller than historical set-up used for field experiment; Jähne, 1993). For our tests this ratio was around 0.07.

What remains to quantify is the quantization error; indeed because of the discrete nature of the image formation system, the image coordinates of each pixel can suffer from quantization errors up to 0.5 pixel, therefore the disparity can be in error as much as 1 pixel. Because of this error, the estimation of the range along the optical axis is inexact, as well along the two directions orthogonal to it. The error along the optical axis dominates (Benetazzo, 2006, Jähne et al., 1994, Rodriguez and Aggarwal, 1990). The quantization error is alleviated by using subpixel (fractional pixel) correspondence. Subpixeling reduces errors depending on the weight function adopted to estimate the cross-correlation map (Nobach and Honkanen, 2005), and has a large impact on the accuracy of the smaller wavelengths (Benetazzo et al., 2012).

An estimation of the quantization error for the stereo system used in his study is obtained through direct 3D computation of a synthetic wavy surface mapped onto the imaged area shown in Fig. 4. Quantization error was then computed through a comparison between the original 3D shape and that one retrieved after applying the stereo method. In this respect, Fig. 12 shows the map of the expected quantization error within the water surface region matched by the stereo cameras. The maximum absolute error is about 3 cm and the root-mean-square error is 1 cm, assuming a factor of 5 as a conservative upper bound for sub-pixel improvement (Benetazzo et al., 2016).

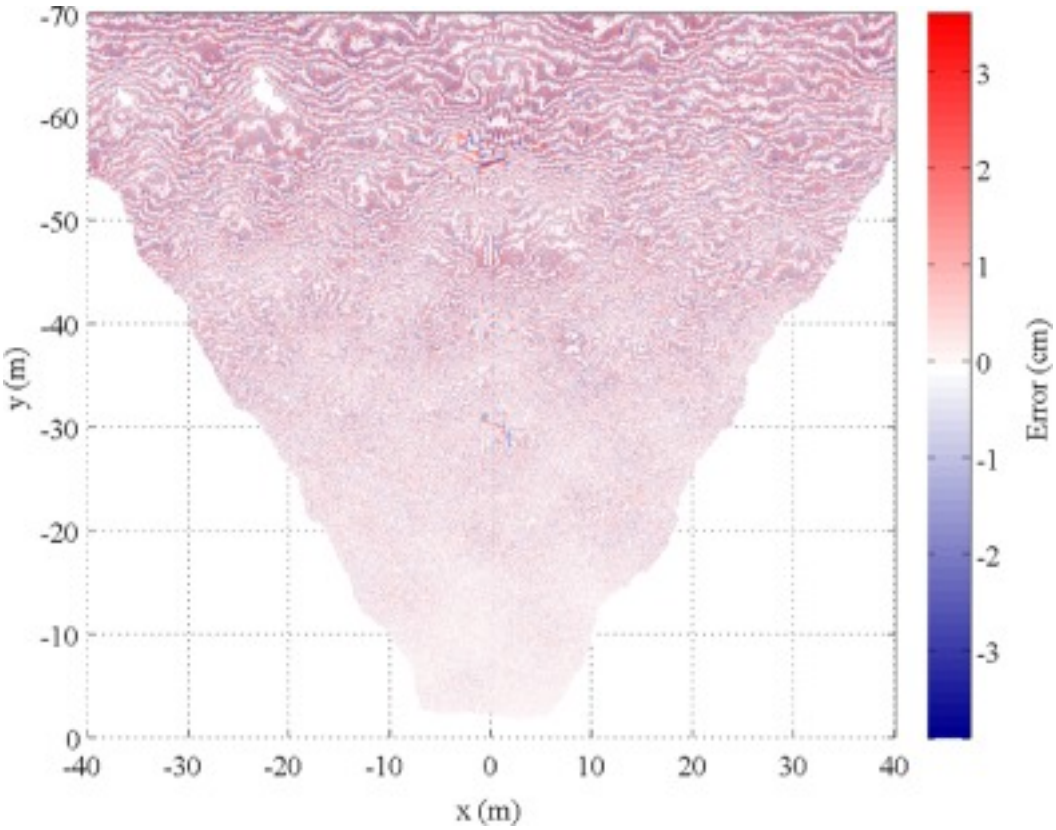

Fig. 12. Map of the quantization error along the vertical axis within the horizontal field of view of the stereo cameras.

To meet requirements of reduced matching and quantization errors we used a modified version (available as free software at http://www.dais.unive.it/wass/) of the dense-stereo algorithm proposed by Hirschmüller (2008), made available within the Open Source Computer Vision (OpenCV) library (Bradski & Kaehler, 2008; http://opencv.org), in order to match (with sub-pixel accuracy) all the pixels of the stereo pair. The semi-global nature of the method has the great advantage that it can relate the photometric consistency of several matching pixels to improve the reliability of the disparity map, especially for areas with loosely distinctive features. As a consequence, we can keep a relatively small window size (13 × 13 pixels) while still obtaining a precise localization of the matches between images. Finally, before being processed for rogue wave detection, time series of sea surface elevations at each position of the *xy*-plane were smoothed using a weighted linear least squares local regression and low-pass filtered at 2.0 Hz.

Appendix C. Sensitivity to the spectral resolution

In this study, extreme sea surface elevations and the surrounding profile have been formulated as a function of the wave spectrum $S(\omega, \theta)$ and its integral moments. This assumption makes the calculation easier to a certain extent, but it requires that the spectrum is available. In this respect, phase-averaged wave numerical models are a routinely and well-consolidated tool used to establish wave conditions around the globe and in regional seas. The variable integrated by this class of models is the directional wave spectrum, which, therefore, may be directly used for the computations described in this study. Nevertheless, for practical applications, the number of frequencies / wavenumbers / directions that discretize the spectrum is generally limited to ease and speed up the computational process. Therefore, 1024 frequencies and 180 directions used to represent the wave spectrum during the experiment with stereo cameras are far from being applicable to the purpose of wave models. Less resolved spectra are generally employed, and here we are interested in verifying to what extent these conditions alter the predictions of the ST and QD models.

We have thus remapped (via linear interpolation; see Fig. 13) the wave spectra shown in Fig. 5 using 36 equally spaced directions, and 40 frequencies geometrically distributed such that $f_{n+1} = 1.1\, f_n$, with $f_1 = 0.05$ Hz and $f_{40} = 2.06$ Hz. The new spectrum has been firstly used for the computation of the parameters required to estimate the probability levels of ST maxima. The expected ST maximum sea surface elevations (both linear and second-order nonlinear) estimated using the subsampled spectrum are very close to those given by the highly-resolved spectrum, with differences smaller than 1%. The differences between spectral moments m_{ijl} are of the same order of magnitude, and for the subsampled spectrum the normalized first minimum of the autocovariance function $\psi 1^* = -0.68$. Most likely the reason for these small changes is that the wave spectra are typically smoothed and continuous, so their integral quantities are slightly modified by a change in resolution (unless the spectral range is abruptly changed). The resampling also slightly affects the sea surface elevations $\eta^{-}1(\tau)$ and $\eta^{-}2(\tau)$ around the maximum crests, which show (Fig. 14) negligible differences when computed with the two differently resolved wave spectra.

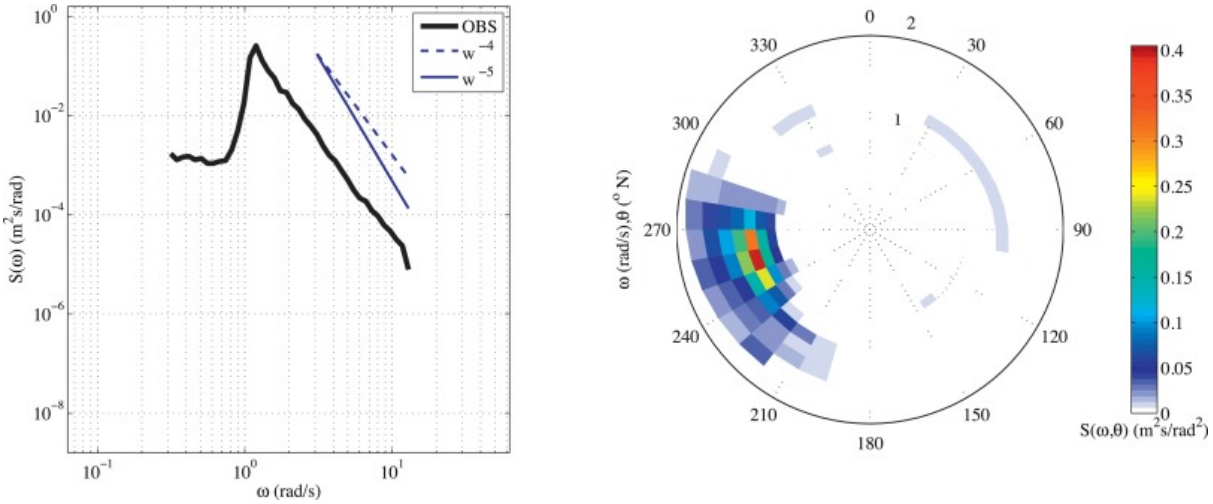

Fig. 13. Subsampling of the observed wave spectra (Fig. 5) using a reduced number of frequencies (for a total of 40 geometrically distributed such that $f_{n+1} = 1.1\, f_n$, with $f_1 = 0.05$ Hz and $f_{40} = 2.06$ Hz) and directions (for a total of 36 equally spaced to cover the full circle). (left panel) Omnidirectional angular frequency wave spectrum estimated from stereo wave data (OBS). The blue dashed and solid lines are reference spectral slopes proportional to ω^{-4} and ω^{-5}, respectively. (right panel) Observed frequency–direction spectrum.

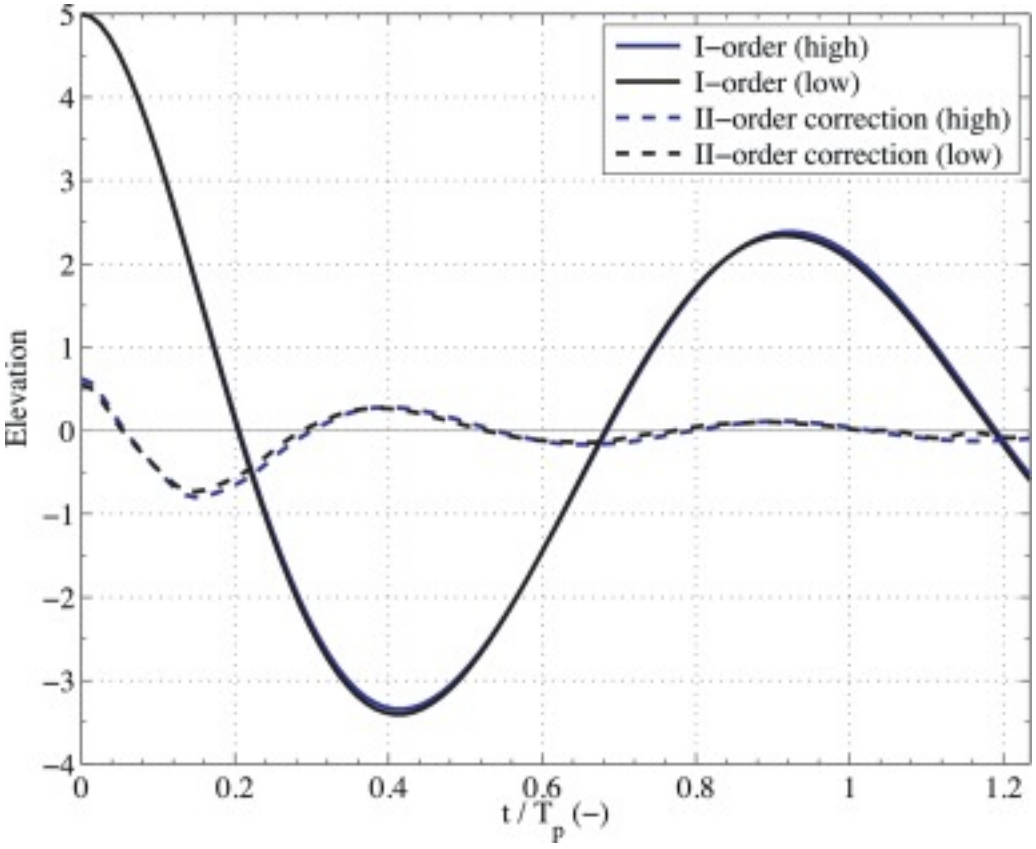

Fig. 14. Linear (I-order) and second-order nonlinear correction (II-order correction) of the temporal shape of the ST wave group elevation at $\boldsymbol{X} = (0, 0)$ near a wave crest with linear height $\eta^{-}1\mathrm{STm} = 1.19H_s$. The profiles are determined using the observed

wave spectra shown in Fig. 5 (high) and Fig. 13 (low). In Figure, the time lag τ is indicated with the time axis t, scaled with T_p, and $t_0 = 0$.

References

T.A.A. Adcock, S. Draper**A note on the variation in shape of linear rogue waves in the ocean** Underw. Technol., 33 (2015), pp. 75-80

T.A.A. Adcock, P.H. Taylor, S. Draper**Nonlinear dynamics of wave-groups in random seas: unexpected walls of water in the open ocean** Proc. R. Soc. A Math. Phys. Eng. Sci., 471 (2015), Article 20150660

T.A.A. Adcock, P.H. Taylor, S. Yan, Q.W. Ma, P.A.E.M. Janssen**Did the Draupner wave occur in a crossing sea?** Proceedingis R. Soc. A, 467 (2011), pp. 1-18

R.J. Adler**The Geometry of Random Fields** John Wiley, New York (USA) (1981), p. 302

R.J. Adler**On excursion sets, tube formulas and maxima of random fields** Ann. Appl. Probab., 10 (2000), pp. 1-74

R.J. Adler, J.E. Taylor**Random Fields and Geometry** Springer, New York (USA) (2007), p. 448

M.A. Alkhalidi, M.A. Tayfun**Generalized Boccotti distribution for nonlinear wave heights** Ocean Eng., 74 (2013), pp. 101-106

F. Arena**On non-linear very large sea wave groups** Ocean Eng, 32 (2005), pp. 1311-1331

M.L. Banner, I.S.F. Jones, J.C. Trinder**Wavenumber spectra of short gravity wave** J. Fluid Mech., 198 (1989), pp. 321-344

F. Barbariol, J.H.G. Alves, A. Benetazzo, F. Bergamasco, L. Bertotti, S. Carniel, L. Cavaleri, Y.Y. Chao, A. Chawla, A. Ricchi, M. Sclavo, H. Tolman**Numerical Modeling of Space-Time Wave Extremes using WAVEWATCH III** Ocean Dyn, 67 (3) (2017), pp. 535-549

F. Barbariol, A. Benetazzo, S. Carniel, M. Sclavo**Space–time wave extremes: the role of metocean forcings** J. Phys. Oceanogr., 45 (2015), pp. 1897-1916

A. Baxevani, I. Rychlik**Maxima for Gaussian seas** Ocean Eng, 33 (2004), pp. 895-911

A. Benetazzo**Measurements of short water waves using stereo matched image sequences** Coast. Eng, 53 (2006), pp. 1013-1032

A. Benetazzo, F. Barbariol, F. Bergamasco, A. Torsello, S. Carniel, M. Sclavo**Observation of extreme sea waves in a space-time ensemble** J. Phys. Oceanogr., 45 (2015), pp. 2261-2275

A. Benetazzo, F. Barbariol, F. Bergamasco, A. Torsello, S. Carniel, M. Sclavo**Stereo wave imaging from a moving vessel: practical use and applications** Coast. Eng, 109 (2016), pp. 114-127

A. Benetazzo, F. Fedele, G. Gallego, P.-C. Shih, A. Yezzi**Offshore stereo measurements of gravity waves** Coast. Eng, 64 (2012), pp. 127-138

P. Boccotti**Some new results on statistical properties of wind waves** Appl. Ocean Res., 5 (1983), pp. 134-140

Boccotti, P., 2000. Wave mechanics for ocean engineering. Oxford, 496 pp.

P. Boccotti, G. Barbaro, V. Fiamma, L. Mannino, A. Rotta**An experiment at sea on the reflection of the wind waves** Ocean Eng, 20 (1993), pp. 493-507

P. Boccotti, G. Barbaro, L. Mannino**A field experiment on the mechanics of irregular gravity waves** J. Fluid Mech., 252 (1993), pp. 173-186

Bradski, G., Kaehler, A., 2008. Learning OpenCV: computer vision with the OpenCV library

L. Cavaleri, A. Benetazzo, F. Barbariol, J. Bidlot, P.A.E.M. Janssen**The Draupner event: the large wave and the emerging view** Bull. Am. Meteorol. Soc. (2017), 10.1175/BAMS-D-15-00300.1

Christou and Ewans, 2014 M. Christou, K. Ewans**Field measurements of rogue water waves** J. Phys. Oceanogr., 44 (2014), pp. 2317-2335

L. Draper**`Freak' ocean waves** Mar. Obs., 35 (1965), pp. 193-195

K. Dysthe, H.E. Krogstad, P. Müller**Oceanic rogue waves** Annu. Rev. Fluid Mech., 40 (2008), pp. 287-310

F. Fedele**Rogue waves in oceanic turbulence** Phys. D Nonlinear Phenom., 237 (2008), pp. 2127-2131

F. Fedele**Space–time extremes in short-crested storm seas** J. Phys. Oceanogr., 42 (2012), pp. 1601-1615

Fedele, F., 2015. On oceanic rogue waves. http://arxiv.org/abs/1501.03370v5

F. Fedele, F. Arena**Weakly nonlinear statistics of high random waves** Phys. Fluids, 17 (2005) Paper No. 026601

F. Fedele, A. Benetazzo, G. Gallego, P.-C. Shih, A. Yezzi, F. Barbariol, F. Ardhuin**Space–time measurements of oceanic sea states** Ocean Model, 70 (2013), pp. 103-115
Fedele et al., 2016

F. Fedele, J. Brennan, Sonia Ponce de León, J. Dudley, F. Dias**Real world ocean rogue waves explained without the modulational instability** Sci. Rep., 6 (2016), pp. 1-11

F. Fedele, G. Gallego, A. Yezzi, A. Benetazzo, L. Cavaleri, M. Sclavo, M. Bastianini**Euler characteristics of oceanic sea states** Math. Comput. Simul., 82 (2012), pp. 1102-1111

F. Fedele, M.A. Tayfun**On nonlinear wave groups and crest statistics** J. Fluid Mech., 620 (2009), pp. 221-239

G.Z. Forristall**Wave crest distributions: observations and second-order theory** J. Phys. Oceanogr. (2000), pp. 1931-1943

J. Gemmrich, C. Garrett**Unexpected waves** J. Phys. Oceanogr., 38 (2008), pp. 2330-2336

E.J. Gumbel**Statistics of Extremes** Columbia University Press (1958), p. 358

N. Hashimoto, T. Nagai, T. Asai**Extension of the maximum entropy principle method for directional wave spectrum estimation** Proceedings of 24th International Conference Coastal Engineering (ACSCE), Kobe (Japan) (1994), pp. 232-246

S. Haver**A possible freak wave event measured at the Draupner Jacket January 1 1995** Proc. Rogue Waves (2004) 20-22 October

H. Hirschmüller**Stereo processing by semiglobal matching and mutual information** IEEE Trans. Pattern Anal. Mach. Intell., 30 (2008), pp. 328-341

L.H. Holthuijsen**Waves in Oceanic and Coastal Waters** Cambridge University Press (2008), p. 387

P.A. Hwang, D.W. Wang, E.J. Walsh, W.B. Krabill, R.N. Swift**Airborne measurements of the wavenumber spectra of ocean surface waves. Part I : spectral slope and dimensionless spectral coefficient** J. Phys. Oceanogr. (2000), pp. 2753-2767

Jähne, B., 1993. Spatio-temporal image processing: theory and scientific applications (Lecture notes in computer science).

B. Jähne, J. Klinke, S. Waas**Imaging of short ocean wind waves: a critical theoretical review** J. Opt. Soc. Amer. A Opt. Image Sci. Vis., 11 (1994), pp. 2197-2209

P.A.E.M. Janssen**Nonlinear four-wave interactions and freak waves** J. Phys. Oceanogr., 33 (2003), pp. 863-884

P.A.E.M. Janssen**On some consequences of the canonical transformation in the Hamiltonian theory of water waves** J. Fluid Mech., 637 (2009), p. 1

C. Kharif, E. Pelinovsky, A. Slunyaev**Rogue Waves in the Ocean** Springer Verlag (2009), p. 21 OMAE2004-51336

G. Lindgren**Some properties of a normal process near a local maximum** Ann. Math. Stat., 41 (1970), pp. 1870-1883

G. Lindgren**Local maxima of Gaussian fields** Ark. Mat., 10 (1972), pp. 195-218

M.S. Longuet-Higgins**On the statistical distribution of the heights of sea waves** J. Mar. Res., 11 (1952), pp. 245-265

M.S. Longuet-Higgins**The effect of nonlinearities on statistical distribution in the theory of sea waves** J. Fluid Mech., 17 (1963), pp. 459-480

M.S. Longuet-Higgins**On the joint distribution of the periods and amplitudes of sea waves** J. Geophys. Res., 80 (1975), pp. 2688-2694

M.S. Longuet-Higgins**Statistical Properties of wave groups in a random sea state** Philos. Trans. R. Soc. London. Ser. A, Math. Phys. Sci., 312 (1984), pp. 219-250

A.K. Magnusson, M.a. Donelan**The Andrea wave characteristics of a measured north sea rogue wave** J. Offshore Mech. Arct. Eng., 135 (2013), pp. 1-10

A.S. Mironov, M.V. Yurovskaya, V.A. Dulov, D. Hauser, C.A. Guérin**Statistical characterization of short wind waves from stereo images of the sea surface** J. Geophys. Res, 117 (2012), p. C00J35

P. Muller, C. Garrett, A. Osborne**Rogue Waves** Oceanography, 18 (2005), pp. 66-75

J.C. Nieto Borge, K. Reichert, K. Hessner**Detection of spatio-temporal wave grouping properties by using temporal sequences of X-band radar images of the sea surface** Ocean Model, 61 (2013), pp. 21-37

H. Nobach, M. Honkanen**Two-dimensional Gaussian regression for sub-pixel displacement estimation in particle image velocimetry or particle position estimation in particle tracking velocimetry**

M. Onorato, A. Osborne, M. Serio, S. Bertone**Freak waves in random oceanic sea states** Phys. Rev. Lett., 86 (2001), pp. 5831-5834

M. Onorato, S. Residori, U. Bortolozzo, A. Montina, F.T. Arecchi**Rogue waves and their generating mechanisms in different physical contexts.**Phys. Rep., 528 (2013), pp. 47-89

V.I. Piterbarg**Asymptotic methods in the theory of Gaussian processes and fields** Translations Math. Monogr. (1996), p. 206

S.O. Rice**Mathematical analysis of random noise** Sel. Pap. Noise Stochastic Processes (1954), pp. 133-294

J.J. Rodriguez, J.K. Aggarwal**Stochastic analysis of stereo quantization error** IEEE Trans. Pattern Anal. Mach. Intell., 12 (1990), pp. 467-470

L. Romero, W.K. Melville**Airborne observations of fetch-limited waves in the gulf of Tehuantepec** J. Phys. Oceanogr., 40 (2010), pp. 441-465

A. Romolo, F. Arena**On Adler space-time extremes during ocean storms** J. Geophys. Res. Ocean., 120 (2015), pp. 3022-3042

E.V. Sanina, S.A. Suslov, D. Chalikov, A.V. Babanin**Detection and analysis of coherent groups in three-dimensional fully-nonlinear potential wave fields** Ocean Model. (2016), pp. 1-14

J.N. Sharma, R.G. Dean**Development and evaluation of a procedure for simulating a random directional second order sea surface and associated wave forces** Ocean Eng. Rep., 20 (1979), p. 112

D. Slepian**On the Zeros of Gaussian Noise** M. Rosenblatt (Ed.), Wiley, New York (1962), pp. 104-115 Time Ser. Anal

H. Socquet-Juglard, K. Dysthe, K. Trulsen, H.E. Krogstad, J. Liu**Probability distributions of surface gravity waves during spectral changes** J. Fluid Mech., 542 (2005), pp. 195-216

M.A. Tayfun**Narrow-band nonlinear sea waves** J. Geophys. Res., 85 (1980), pp. 1548-1552

M.A. Tayfun**On narrow-band representation of ocean waves 1** Theory. J. Geophys. Res., 91 (1986), pp. 7743-7752

M.A. Tayfun, F. Fedele**Wave-height distributions and nonlinear effects** Ocean Eng, 34 (2007), pp. 1631-1649

D.a.G. Walker, P.H. Taylor, R.E. Taylor**The shape of large surface waves on the open sea and the Draupner New Year wave** Appl. Ocean Res., 26 (2004), pp. 73-83

K.J. Worsley**The geometry of random images** Chance, 9 (1996), pp. 27-40

WW3DG, 2016. The WAVEWATCH III® Development Group (WW3DG), 2016: User manual and system documentation of WAVEWATCH III® version 5.16. Tech. Note 329, NOAA/NWS/NCEP/MMAB, College Park, MD, USA, 326 pp. + Appendices.